Chapter 5

Photocatalytic Production of H_2 on Nanocomposite Catalysts

Sections reprinted with permission from Ryu, S.Y.; Choi, J.; Balcerski, W.; Lee, T.K.; Hoffmann, M. R. *Industrial & Engineering Chemistry Research* **2007**, *46*, 7476.

Abstract

The photocatalytic production of H_2 in water with visible light using nanocomposite catalysts, which include Q-sized CdS, CdS nanoparticles embedded in zeolite cavities (CdS/Zeolite), and CdS quantum dots (Q-CdS) deposited on $KNbO_3$ ($CdS/KNbO_3$ & $Ni/NiO/KNbO_3/CdS$), are investigated. The rate of H_2 production in alcohol/water mixtures and other electron donors at $\lambda \geq 400$ nm is the highest with the hybrid catalyst, $Ni/NiO/KNbO_3/CdS$ with a measured quantum yield, ϕ, of 8.8%. The relative order of reactivity as a function of catalyst is $Ni(0)/NiO/KNbO_3/CdS$ > $Ni(0)/KNbO_3/CdS$ > $KNbO_3/CdS$ > $Ni/KNbO_3$ > CdS/NaY-Zeolite > TiY-Zeolite > CdS, while the reactivity order with respect to the array of electron donors is 2-propanol > ethanol > methanol > sulfite > sulfide > H_2O. In addition, the rates of H_2 production from water and water-alcohol mixtures are correlated with fluorescent emission spectra and fluorescence lifetimes. Irradiation of $Ni/NiO/KNbO_3/CdS$ proceeds via the partial reduction of Cd(II) to Cd(0) on surface of CdS. The coupling of Ni(0)/NiO and Cd(0) on the surface of $KNbO_3$ appears to some of chemical principles a Ni/Cd battery at high overvoltages. Evidence for the formation of nickel hydride as an important intermediate has been obtained.

Introduction

The production of hydrogen from the splitting of water via photocatalysis has been achieved with a variety metal oxide semiconductors such as TiO_2 [1-3], $SrTiO_3$ [4], $BaTi_4O_9$ [5], $RbPb_2Nb_3O_{10}$ [6], and $Na_2Ti_6O_{13}$ [7]. However, the majority of the simple and mixed-metal oxides photocatalysts are primarily active for H_2 production under UV irradiation ($\lambda <$ 385 nm or $E_{bg} \geq 3.0$ eV). More recently, there has been a focused effort on the development of photocatalysts that are capable of using visible light (λ = 400–700 nm) for the photocatalytic production of H_2.

Hydrogen production from water using semiconductor photocatalysts[8-11] has attracted considerable interest since the pioneering work of Fujishima and Honda[12], who discovered that water can be photo-electrochemically decomposed into hydrogen and oxygen using a semiconductor (TiO_2) electrode under UV irradiation. Since 1972, a large number of metal oxides and sulfides (TiO_2, CdS, ZnO, ZrO_2, titanates, niobates, and tantalates) have been reported to have photocatalytic activity for splitting water[13].

$$2\,H_2O \xrightarrow{\text{UV \& visible light}} 2\,H_2 + O_2 \qquad (5.1)$$

The overall multi-electron redox potentials for the multi-electron reactions at pH 7 suggest that H_2 production with the input of UV-visible light energy is feasible.

$$H_2O \longleftrightarrow H^+ + OH^- \qquad (5.2)$$

$$2\,H_2O + 2\,\bar{e} \longleftrightarrow H_2 + 2\,{}^{-}OH \qquad (5.3)$$

$$2\,H_2O \longleftrightarrow O_2 + 4\,H^+ + 4\,\bar{e} \qquad (5.4)$$

The redox potential for reaction 5.1 at pH 7 is E_H = -1.23 V (NHE) with the corresponding half-reactions of -0.41 V (eq. 5.3) and 0.82 V (eq. 5.4), which gives a ΔG^o = +237 kJ/mole)[13]. However, with the input of light at wavelengths ≤ 1000 nm (i.e., 1.23

eV ≈ 1000 nm), the overall energy requirement for the photosynthetic splitting of water can be met with solar radiation in principle. On the other hand, the rate of reaction in the normal Marcus regime should depend on the overall driving force (i.e., lower wavelength irradiation is preferable kinetically) and the thermodynamics of the initial or sequential one-electron transfer processes at the semiconductor surfaces. Moreover, the one-electron transfers[14] (eqs. 5.5–5.7) are much less favorable thermodynamically than the overall two-electron transfer reactions as shown below:

$$H^+ + e^-_{aq} \xrightleftharpoons{E_H = -2.5\ V\ (pH\ 7)} H^{\cdot}_{aq} \tag{5.5}$$

$$H_2O \xrightleftharpoons{E_H = -2.3\ V\ (pH\ 7)} {}^{\cdot}OH + H^+ + e^-_{aq} \tag{5.6}$$

$${}^{-}OH \xrightleftharpoons{E_H = -1.8\ V\ (pH\ 0)} {}^{\cdot}OH + e^-_{aq} \tag{5.7}$$

CdS, an n-type semiconductor with E_g = 2.4 eV, has been shown to have photocatalytic activity for H_2 production under visible light irradiation [15-18], although, sacrificial electron donors[19] such as C_2H_5OH [20], HS^- [18,21,22] or SO_3^{2-} [16] are used to obtain measurable rates of H_2 production and to avoid the photocorrosion of CdS in the presence of O_2.

In order to enhance the photocatalytic activity of CdS, efforts have been made to combine CdS with other semiconductors having different band energies (e.g., TiO_2/CdS[23], ZnO/CdS, ZnS/CdS[24,25], $K_4Nb_6O_{17}$/CdS[26], or $K_2Ti_4O_9$/CdS composites[27,28]). An alternative approach to enhance the photoactivity of CdS is to couple CdS with mesoporous or macroreticular materials to form hybrid or composite photocatalysts[29-46]. In these cases, the photogenerated electrons in CdS are able to move freely into an attached semiconductor or a framework of porous molecules, while the photo-generated

holes are trapped in CdS. Charge separation reduces the frequency of charge recombination, and thus improves the net photocatalytic activity of CdS.

The electronic levels of nanoparticulate or Q-CdS can be tuned by changing or controlling particle size without changing the chemical composition. For example in the case of nanoparticulate ZnO, Hoffmann and co-workers[47,48] reported a tenfold increase in photoefficiency for the photocatalytic production of hydrogen peroxide with a decrease in particle size from 40 to 23 nm. In another example, Hoffman et al.[49,50] found an increase in quantum efficiency for photo-polymerization of methylmethacrylate with a corresponding decrease in particle size using Q-CdS.

In this paper, we report on the synthesis of and optimization of hybrid CdS/Zeolite and CdS/$KNbO_3$ nanocomposite catalysts that are effective for H_2 production in aqueous suspension.

Experimental

Nanoparticulate CdS was synthesized according to the methods described previously by Hoffmann and co-workers[49] while CdS/Zeolite nanocomposites were synthesized starting with commercially available NaY-Zeolite (Si/Al=6) (Strem Chemicals, Inc.). Nanoparticulate CdS was prepared within the pore structure of NaY-Zeolite by first exchanging Na^+ with Cd^{2+}, followed by *in situ* reaction with HS^- which was formed by the dissolution Na_2S[51] crystals in 95% ethanol in a Vacuum Atmospheres® glove box. In this procedure, 1.0 g of NaY zeolite was mixed into 20 ml of 0.01 M solution of cadmium acetate in ethanol. Na^+ was exchanged with Cd^{2+} for 24 hr at 25°C with continuous mixing. After ion exchange was complete, 20 mL of a sodium sulfide solution (0.01 M)

was added drop wise to the CdY-Zeolite suspension resulting in the formation of CdS on the internal and external surfaces of the zeolite matrix. The nanocomposite material was filtered and washed with ethanol for multiple cycles.

TiY zeolite was obtained by mixing an aqueous solution of ammonium titanyl oxalate[52,53] with HY-Zeolite. In a preliminary step, HY-Zeolite was obtained by ion exchange of the NaY-Zeolite with a 0.1 M NH_4Cl. After rinsing with H_2O, HY-Zeolite was calcined at 500 °C for 15 h, with an initial temperature ramp of 200°C/hour. Sample cooling was performed at same decreasing rate. The mole fraction of Ti(IV) incorporated into the HY-Zeolite was determined by analytical difference before and after treatment $\left(\Delta n_{Ti} = \left(n^{o}_{Ti} - n^{f}_{Ti}\right)\right)$. Ti(IV)-Zeolite was repeatedly washed with water to remove any residual species adsorbed on exposed surfaces and then dried in an oven. After an initial low-temperature drying phase, the sample was calcined at 450 to 500 °C for 8 hours. The preparative procedure for CdS/TiY-Zeolite was analogous to that for CdS/NaY-Zeolite (*vide supra*).

Stoichiometric ($KNbO_3$)[54] and non-stochiometric potassium niobate ($KNb_{1.5}O_{4.25}$)[55] were prepared via high temperature solid-state reactions between K_2CO_3 and Nb_2O_5 as functions of calcination temperature and mole ratio of Nb_2O_3 to K_2CO_5.

$$K_2CO_3 + Nb_2O_5 \xrightarrow{\Delta} 2\ KNbO_3 + CO_2 \qquad (5.8)$$

Powdered K_2CO_3 and Nb_2O_5 were mixed together with constant grinding in a mortar at a mole ratio of 1.0 to 1 of Nb_2O_5:K_2CO_3. After thorough mixing and grinding to reduce particle size, the powdered mixture was pressed into a pellet at 27.6 Mpa and then heated at 925 ^{o}C for 10 hr with a heating and cooling temperature ramp of ±200 ^{o}C. The X-ray diffraction pattern confirmed $KNbO_3$. With slight variations of the Nb_2O_5 to

K_2CO_3 mole ratio and the actual temperature of solid state synthesis, $K_4Nb_6O_{17}$ (T ~ 1125 ^oC) or a mixture of $KNbO_3$ and $K_4Nb_6O_{17}$ (T ~ 1125 ^oC) are obtained. Elemental nickel and NiO coated $KNbO_3$ powders were obtained by first treating the pure $KNbO_3$ sample with $Ni(NO_3)_2$ in a water suspensions for 1 day, filtered, washed and dried.. After ion-exchange with Ni^{2+} the Ni(II)/$KNbO_3$ sample was reduced in a H_2 atmosphere at 500 ^oC for 2 hr. This was followed by partial oxidation in an O_2 atmosphere at 200 ^oC for 1 hr to form NiO on the surface of $KNbO_3$. Following the latter procedure, CdS nanoparticles were deposited by mixing the Ni/NiO/$KNbO_3$ powder with a cadmium acetate solution in ethanol for 1 day and then mixing in Na_2S and allowing the formation of CdS for 7 days before filtration, washing and subsequent drying X-ray diffraction patterns for $KNbO_3$ and its nanocomposites gave 2θ peaks that correspond to peaks reported for pure $KNbO_3$.

Diffuse reflectance and absorption spectra were recorded by using a Shimadzu UV-2101PC with an integrating sphere attachment (Shimadzu ISR-260). Steady-state fluorescence spectra were collected on a Hitachi F-2500 fluorometer with samples excited at 400 nm.

Photoluminescence lifetimes in solution were measured with a streak camera (Hamamatsu, Streak Scope C4334) after excitation with the second-harmonic (430 nm) of an amplified femtosecond mode-locked Ti:Sapphire laser. The sample solution was put into a quartz cell (1 cm × 1 cm), and the fluorescence emission was focused into the streak camera through a cutoff filter (< 530 nm) at a 90° angle with respect to the excitation beam.

DRIFT spectra were acquired using a Bio-Rad FTS-45 FTIR spectrometer with a liquid N_2-cooled MCT detector at 4 cm^{-1} resolution using a Spectra-Tech Collector

diffuse-reflectance accessory. Solid samples were held in the diffuse reflectance accessory in the sample cup of a Spectra-Tech high temperature environmental chamber (HTEC). The sample could be resistively heated to 1000 K (± 1 K) and the chamber evacuated to 1 μTorr. Gases and vapors can be introduced through a separate port via a manifold.

Photolysis experiments were performed by using the collimated output of a high-pressure 500 W Hg-Xe arc lamp as a light source in combination with 400 nm cut-off filter. The incident light flux per unit area, I_0, was measured with a potassium ferrioxalate actinometer as 4.65×10^{15} photons cm^{-2} $s^{-1.}$ All samples were purged with Ar gas for 30 min before photolysis in order to eliminate O_2. The amount of H_2 evolved during photolysis was analyzed using gas chromatography (HP G1800A) with TCD. Nitrogen was used as the carrier gas and the separations were achieved with a molecular sieve column (30 m × 0.32 mm × 12.00 μm). Calibration curves were linear over a broad range of H_2 concentrations in He.

Results

Nanoparticulate CdS colloids were synthesized in four different solvents by rapidly mixing of Na_2S solutions into cadmium acetate solutions[49,56-59] under anoxic conditions. This resulted in an immediate precipitation of small crystallites. In mixed solvent system, where the pH of the colloidal suspension of CdS was close to 8, the colloidal CdS suspension were stabilized by the net negative charges on particle surfaces (i.e., $pH_{solv} > pH_{zpc} = 2.0$)[60-63]. The mean particle diameter of the CdS colloids synthesized in ethanol was 4 nm as determined by TEM while the relative size of the CdS particles in

suspension was estimated from the band-gap energies obtained from the UV-vis absorption spectra of the transparent colloidal suspensions. The equilibrium particle size in the CdS solvent suspensions was dependent on the viscosity of solvent and on the temperature of synthesis as reported previously by Hoffman et al.[64]

Cadmium sulfide was synthesized within the pore spaces of the aluminosilicate zeolites (Si:Al = 6:1, NaY zeolite)[65-72] by the direct reaction of sorbed Cd^{2+} with the aqueous Na_2S. The zeolite support, which serves as a mesoporous host material, is used to control CdS particle size and stability. The size of CdS colloids are constrained, in part, by the cavity size of the particular zeolite support. In addition, the zeolite framework should inhibit Ostwald ripening (i.e., continued particle growth).

However, formation of CdS clusters or particles may not occur exclusively within the cavities or pores of the zeolite. A fraction of the formed CdS may have precipitated on the external surfaces of NaY-Zeolite, although, the XRD patterns of NaY-Zeolite with embedded CdS were consistent with that of NaY zeolite alone without discernable 2θ peaks for CdS. This result indicates that the inherent framework structure of NaY-Zeolite was maintained after ion-exchange, and that CdS was synthesized preferentially within the NaY-Zeolite cavities.

The UV-vis absorption spectra of CdS colloids, which were measured at room temperature, had spectral features that were consistent with our previous results.[64] The corresponding the fluorescence spectra (λ_{ex} = 380 nm) of the CdS colloids in H_2O and ethanol are shown in Figure 5.1. The emission bands for CdS in ethanol were observed at λ_{em} = 554, whereas a much weaker emission band was observed at λ_{em} = 633 nm for colloidal, Q-sized CdS suspended in H_2O. The fluorescence spectra were characterized

by large red-shifted emissions, indicating radiative relaxations from surface trapping states[73]. The relative differences in the photoluminescence response can be attributed to interactions between the surface of CdS and the solvent.

In the case of ethanol, the emission intensity increases (Figure 5.2) with a corresponding blue shift in wavelength as the V_{EtOH}/V_{H_2O} ratio increases. The responses as a function of the mole fraction of ethanol, χ_{EtOH}, suggest a relatively strong interaction of ethanol at the charged surface of CdS.

Ethanol can act as a potential electron donor to the valence band hole, h^+_{vb} , or a trapped hole, h^+_{tr},

$$C_2H_5OH \longleftrightarrow CH_3CHO + 2H^+ + 2\bar{e} \quad (E^0_{H,\,pH\,7} = 0.22\ V) \tag{5.9}$$

$$C_2H_5OH + > h^+_{tr}\ (> CdSH^{+\cdot} \text{ or } > CdOH^{+\cdot}) \longrightarrow CH_3\dot{C}HOH + > H \tag{5.10}$$

Furthermore, ethanol can modulate the thickness of the electrical double layer surrounding charged CdS in water. The surface interaction of ethanol with CdS is clearly demonstrated by the increase in the fluorescence intensity with a corresponding increase in the mole fraction of ethanol, χ_{EtOH} (*vide supra*). When sulfite (HSO_3^- and SO_3^{2-}) is substituted for ethanol as an electron donor, similar increases in fluorescence intensity coupled with shifts in λ_{em} from 633 nm to 645 nm are observed (Figure 5.3).

The fluorescence emission intensities can be correlated with the fluorescence lifetimes, which, in turn, depend on the dielectric constant of the solvent[74]. In the case of Q-CdS, the fluorescence lifetime was determined to be 2.5 ns in neat ethanol, 0.5 ns in ethanol-water (V_{EtOH}/V_{H_2O} = 1:1), and to 20 ps in pure water.

The diffuse reflectance and emission spectra of CdS embedded in NaY-Zeolite

showed distinctly different behavior than those observed for the Q-CdS in EtOH (Figure 5.4). The absorption band edged of CdS/NaY-Zeolite at 524 nm is red-shifted, whereas the emission band at λ_{em} = 526 nm is blue-shifted relative to the transparent Q-CdS colloids in EtOH. The shift in the diffuse reflectance spectrum should depend on the size and structure of the embedded colloids or clusters within NaY-Zeolite cavity. Red-shift is most likely due to the formation of CdS clusters in the restricted space of the zeolite cavities (d ~1.3 nm) as opposed to the formation of crystalline cubic or hexagonal CdS (e.g., Hawleyite or Greenockite, *vide supra*)[70-72,75,76]. As a consequence, the cavity-bound CdS clusters have very small Stokes shifts[77-81], $\Delta\lambda$ (i.e., $\lambda_{ex} - \lambda_{em}$).

The rates of H_2 evolution were determined from apparent zero-order $[H_2]$ versus time profiles under an argon atmosphere to minimize oxidative photocorrosion [46,82,83] and subsequent dissolution[84-88]. Typical profiles $[H_2]$ vs. time plots (Figure 5.5) for photolysis of transparent Q-sized CdS colloids indicates a strong inverse pH dependence [89]. Furthermore, the rate of H_2 production is dependent on the ethanol-to-water volume ratio as shown in Figure 5.6. The rate, $d[H_2]/dt$, appears to be the highest in the V_{EtOH}/V_{H_2O} range of 1:3 (EtOH:H_2O). However, the photoluminescence suggests that $d[H_2]/dt$ should increase as V_{EtOH}/V_{H_2O} increases. In contrast, the H_2 production rate is marginal at pH 8 in the absence of an alternative electron donor, while at the other end of the V_{EtOH}/V_{H_2O} spectrum (i.e., pure EtOH with a trace of H_2O= 0.001 M) the linear H_2 production rate was approximately 1/3 of the maximum $d[H_2]/dt$.

The rates of H_2 production for the CdS-Zeolite nanocomposites, CdS/NaY-Zeolite and CdS/TiY-Zeolite, at a V_{EtOH}/V_{H_2O} of 1: 3, are compared to those obtained with Q-CdS

alone in Figures 5.7 and 5.8. The impact of increasing ionic strength on the rate of H_2 production is illustrated in Figure 5.8. The corresponding rates of H_2 production with the $KNbO_3$ composites are shown in Figures 5.9 and 5.10.

Apparent quantum yields, ϕ, for H_2 production, were determined as follows:

$$\phi = \frac{\frac{dm_{H_2}}{dt}}{I^o_{abs}} \tag{5.11}$$

where dm_{H_2}/dt is an initial production rate of H_2 (mol s^{-1}) and I^o_{abs} photon absorption rate of Q-size CdS colloids in units of Einstein s^{-1} ($mol(e^-)\,s^{-1}$). The light absorbed directly by the transparent Q-CdS, ($I^{CdS}_{abs} = I_o\left(\left(I_o - I_t\right)/I_o\right)A$), was determined from the measured incident photon flux, I_0, in units of photons cm^{-2} s^{-1}, the exposed reactor cross section, A = 74.9 cm^2, the fraction of incident light absorbed by CdS where I_t is the transmitted photon flux, and I_0 = 4.65 x 10^{15} photons/cm^{-2} s^{-1} as determined by ferrioxalate actinometry [90].

The specific light absorption rate determined for the transparent Q-CdS colloids is more precise that obtained for the CdS-Zeolite and $KNbO_3$/CdS composites due to differences in light scattering related to their larger particle sizes. In the case of the Q-CdS colloids, I^{CdS}_{abs} is determined by taking the difference of the light fluxes measurements determined at front and back of the photoreactor cell with ferrioxalate actinometer[91]. Scattered light from the photoreactor is negligible for Q-CdS nanoparticulate suspensions which were transparent (i.e., average particle diameter << λ_{hv}). For the CdS colloids, the fraction of absorbed light, (1 - I_t /I_0), was measured as 42.3 (± 2.1)% for a CdS concentration of 2.0 × 10^{-5} M. From the combined measurements of the H_2 mass

production rate in moles per second and the specific light absorption rate, the quantum yield for the CdS colloids was measured as $\phi = 0.12$ %.

Using a similar procedure, the quantum yields for CdS-Zeolite and CdS/$KNbO_3$ composites were determined as described above, except that the amount of light scattered from nanocomposites zeolite suspension was factored into account by the methods of Cornu et al.[92,93]. In this approach, the absorbed light flux is given by

$$I_{abs} = \left[I_0 - \left(I_B + I_S \right) \right] \tag{5.12}$$

where I_B is light flux measured behind the photoreactor (e.g., ferrioxalate actinometry), and I_s denotes the total scattered light including back-scattered, side-scattered, and forward-scattered light. For the nanocomposites suspensions, I_a was measured as 1.90×10^{15} photons cm^{-2} s^{-1}, and the corresponding quantum yields for the CdS/NaY-Zeolite and Ni/NiO/$KNbO_3$/CdS composite of determined to be 0.5 % and 8.8%, respectively, for visible light irradiation ($\lambda \geq 400$ nm).

In Figure 5.10, we compare irradiations of Ni/NiO/$KNbO_3$/CdS suspensions at $\lambda \geq 300$ nm and $\lambda \geq 400$ nm to the Ni-free $KNbO_3$/CdS composite. These results show that $KNbO_3$/CdS was active in the UV range, while the 4-way composite, Ni/NiO/$KNbO_3$/CdS at 0.1 wt% Ni was active in both the UV and visible portions of the spectrum. The highest H_2 production rates were obtained with a Ni-deposition level of 0.1 wt% as ($Ni_T = Ni^o + NiO$) shown in Figure 5.11. The corresponding shifts in the absorption spectra for $KNbO_3$ and its composites are shown in Figures 5.12 and 5.13 as functions of the weight percent loadings of Ni and CdS, respectively.

The rate of H_2 production on the four-component composite, Ni(0)/NiO/$KNbO_3$/CdS, is compared to the three-component composite containing only elemental nickel,

Ni(0)$KNbO_3$/CdS, in Figure 5.14. The Ni(0)/NiO/$KNbO_3$/CdS composite production is linear over many hours while the Ni(0)$KNbO_3$/CdS composite shows non-linear behavior over the same timeframe. The relative effects of the isopropanol (IPA), ethanol (EtOH), and methanol (MeOH) on H_2 production for $KNbO_3$/CdS at $\lambda > 400$ nm are shown in Figure 5.15. In this case, the order of reactivity is IPA > EtOH > MeOH, which is in inverse order of their dielectric constants (i.e., $\varepsilon_{IPA} = 19 < 24.3 < 33 = \varepsilon_{MeOH}$). The relative hydrogen production rates are summarized in Table 5.1.

It should be noted that dramatic color changes take place during photolysis of the Q-CdS and the CdS nanocomposite materials. In all cases, the suspensions are yellow before illumination (note: the NaY-Zeolite and $KNbO_3$ powders are white before deposition of CdS). However, very quickly after exposure to a focused beam of light at $\lambda \geq 400$ nm, the color changes very quickly to a silver gray. As the color changes from yellow to gray, H_2 production is observed as a steady stream of gas bubbles rising up in the photolysis cell. After the light is removed and the gas-tight reactor is opened to air, the solid samples slowly revert to a yellow color after approximately two hours exposure to oxygen.

Discussion

The experimental results for CdS and the CdS composite systems clearly show that the nature of the electron donor plays an important role in determining the photophysical and photochemical properties. The fluorescent emission intensities as shown in Figures 5.1-5.3 are clearly enhanced in the presence of the electron donors, C_2H_5OH and HSO_3^-/SO_3^{2-}.

The emissive state appears to lie in a shallow trapping state, which is energetically located between conduction band (CB) and valence band (VB) edges. During the fluorescence excitation, the photogenerated electron, which has been promoted to the excited state (CB), undergoes a very fast non-radiative relaxation to the emissive state (i.e., a shallow trapping state), following a radiative relaxation back to the VB (emission). Ethanol and sulfite which have been added as VB electron donors interact strongly at the CdS surface and provide electron density to surface trapped holes. This has the effect of retarding electron-hole recombination, increasing the fluorescence lifetime, and increasing the measured fluorescence intensity.

In an early study with nano-particulate ZnO, we[47] observed an increase in the steady-state fluorescence intensity with a corresponding increase in electron acceptor concentration (i.e., a strong increase in emission intensity with a increase in the oxygen partial pressure) or donor, depending on the nature of the surface interaction and the ability of the acceptor or donor function as a surface-bound electron- or hole-trap. We also noted that the fluorescence quenching of various cations or anions depended strongly on the surface charge characteristics of the ZnO colloids as a function of pH. Similar effects can be invoked in the case of quantum-sized CdS.

The net surface charge on the CdS colloids arises due to chemical interactions [60,62,63,94] at the interface, which are initiated by the hydrolysis of the near surface layer of CdS to form surface functionalities that are dominated by cadmium mercapto group, >CdSH, and cadmium hydroxyl, >CdOH functionalities as follows:

$$\left[\begin{matrix} S^{2-} \\ Cd^{2+} \end{matrix} > (CdS) \right]_2 + H_2O \xrightleftharpoons{K_H} \begin{matrix} S^{2-} \\ Cd^{2+} \end{matrix} > Cd(II)SH + \begin{matrix} S^{2-} \\ Cd^{2+} \end{matrix} > S(-II)Cd(II)OH \qquad (5.13)$$

The variable surface charges arise from protonation and deprotonation of surface sulfhydryl and hydroxyl groups as depicted in eqs. 5.14 to 5.19.

$$\begin{matrix} S^{2-} \\ Cd^{2+} \end{matrix} > CdSH \; + \; H^+ \rightleftharpoons \begin{matrix} S^{2-} \\ Cd^{2+} \end{matrix} > CdSH_2^+ \tag{5.14}$$

$$\begin{matrix} S^{2-} \\ Cd^{2+} \end{matrix} > CdSH_2^+ \overset{K_{a1}^s}{\rightleftharpoons} \begin{matrix} S^{2-} \\ Cd^{2+} \end{matrix} > CdSH \; + \; H^+ \tag{5.15}$$

$$\begin{matrix} S^{2-} \\ Cd^{2+} \end{matrix} > CdSH \overset{K_{a2}^s}{\rightleftharpoons} \begin{matrix} S^{2-} \\ Cd^{2+} \end{matrix} > CdS^- \; + \; H^+ \tag{5.16}$$

$$\begin{matrix} S^{2-} \\ Cd^{2+} \end{matrix} > CdOH \; + \; H^+ \rightleftharpoons \begin{matrix} S^{2-} \\ Cd^{2+} \end{matrix} > CdOH_2^+ \tag{5.17}$$

$$\begin{matrix} S^{2-} \\ Cd^{2+} \end{matrix} > CdOH_2^+ \overset{K_{a1.1}^s}{\rightleftharpoons} \begin{matrix} S^{2-} \\ Cd^{2+} \end{matrix} > CdOH \; + \; H^+ \tag{5.18}$$

$$\begin{matrix} S^{2-} \\ Cd^{2+} \end{matrix} > CdOH \overset{K_{a2.1}^s}{\rightleftharpoons} \begin{matrix} S^{2-} \\ Cd^{2+} \end{matrix} > CdO^- \; + \; H^+ \tag{19}$$

The surface chemistry of hydrated CdS is complicated further by adsorption of chemical species present in the background electrolyte, Cd^{2+} and HS^-. For example, HS^- is often used as a sacrificial electron donor[33] for the photocatalytic production of H_2 and Cd^{2+} has been added in excess[95] in attempts to enhance the photochemical reactivity of CdS. As mentioned above, Henglein[59] has noted that the photophysical properties of CdS colloids are strongly influence by excess hydroxide ion.

In the simplest case, at low ionic strength in the absence of added cations or anions, the isoelectric point or 'point of zero charge' is described as follows in terms of the concentrations of the relevant surface species as a function of pH:

$$\left[\begin{matrix} S^{2-} \\ Cd^{2+} \end{matrix} > CdSH_2^+ \right] + \left[\begin{matrix} S^{2-} \\ Cd^{2+} \end{matrix} > CdOH_2^+ \right] = \left[\begin{matrix} S^{2-} \\ Cd^{2+} \end{matrix} > CdS^- \right] + \left[\begin{matrix} S^{2-} \\ Cd^{2+} \end{matrix} > CdO^- \right] \tag{5.20}$$

Park and Huang [94] have argued that, in addition to the surface functional groups defined by the equilibria of eqs. 13-19, that the sites depicted by $\left[\begin{matrix} S^{2-} \\ Cd^{2+} \end{matrix} > CdS^- \right]$ and

$\left[\begin{matrix} S^{2-} \\ Cd^{2+} \end{matrix} > CdO^{-} \right]$ will be involved in surface complexation or chemisorption reactions with other potential determining species in solution, such as Cd^{2+} and HS^{-}, when those species are in excess beyond the background concentrations arising from the equilibrium dissolution of CdS[96]:

$$CdS_{(s)} + H^{+} \underset{H_2O}{\overset{K_{sp}}{\rightleftharpoons}} Cd^{2+} + HS^{-} \quad (\log K_{sp} = 14.4) \tag{5.21}$$

Additional surface reactions, which will influence the overall charge on the CdS, include:

$$\begin{matrix} S^{2-} \\ Cd^{2+} \end{matrix} > CdS^{-} + Cd^{2+} \rightleftharpoons \begin{matrix} S^{2-} \\ Cd^{2+} \end{matrix} > CdSCd^{+} \tag{5.22}$$

$$\begin{matrix} S^{2-} \\ Cd^{2+} \end{matrix} > CdO^{-} + HS^{-} \rightleftharpoons \begin{matrix} S^{2-} \\ Cd^{2+} \end{matrix} > Cd < \begin{matrix} SH^{-} \\ O^{-} \end{matrix} \tag{5.23}$$

In addition to the equilibrium dissolution of CdS, we must also consider dissociation of the diprotic H_2S in terms of the following acid equilibria[97-103]:

$$H_2S \underset{H_2O}{\overset{K_{a1}}{\rightleftharpoons}} H^{+} + HS^{-} \tag{5.24}$$

$$HS^{-} \underset{H_2O}{\overset{K_{a2}}{\rightleftharpoons}} H^{+} + S^{2-} \tag{5.25}$$

where $pK_{a1} = 7.0$ and $pK_{a2} = 17.4$.

For a fixed concentration of $[Cd^{2+}]$ at $pH < pK_{a1}$, the surface charge on CdS is a function of the solution pH as follows[104]:

$$\sigma_0 \Big|_{[Cd^{2+}]=\text{const}} = \frac{\partial \sigma_0}{\partial pH} \Big|_{pH \neq pH_{zpc}} \left(pH - pH_{zpc} \right) \tag{5.26}$$

Park and Huang[104] determined a pH of zero point of charge, pH_{zpc}, of 7.5 using electrophoretic mobility measurements and acid-base titrations. At an ionic strength of μ = 0.05 M, they determined $pK_{a1}^{s} = 6.1$ and $pK_{a2}^{s} = 9.0$ for $[Cd^{2+}]$ = 2.5 μM and σ_0 = 20 mC cm^{-2}.

In contrast, other researchers [60,62,63] have reported substantially lower values for the pH_{zpc} for CdS in aqueous suspensions. Under experimental conditions that were quite different from those employed by Park and Huang[104], Nicolau et al.[63] determined a pH_{zpc} = 1.8 for 0.01 M Na_2SO_4 and KCl as background electrolytes based on electrophoretic mobility measurements, although in the presence of added $CdCl_2$ found additional isoelectric points at pH = 8.8, 7.8, and 7.1, respectively, as the Cd^{2+} was increased from 10^{-4} to 10^{-3} to 10^{-2} M. Parks [105] reported a pH_{zpc} = 10.4 for CdO (i.e., $>CdOH_2^+, >CdOH, >CdO^-$) which would correspond to the surface equilibria of eqs. 17-19. In a follow-up study, Liu and Huang[62] reported a pH_{zpc} for cubic CdS (Hawleyite) of 7.0, which can be compared to their reported value for hexagonal CdS (Greenockite) of 7.5.

Guindo et al.[61] found even lower values of pH_{zpc} between 1 and 1.5 for spherical CdS particles prepared by the method of Matijevic and Wilhemy[106]. However, they pointed out that the IEP (isoelectric point) was sensitive to the specific surface characteristics of CdS that depend on the degree of oxidation or aging as noted by the shift in IEP to higher values for samples that were synthesized over longer periods of time.

The interaction of the various electron donors with the charged CdS surface will also depend on their chemical and physical properties. For example, we can compare water and ethanol as electron donors. Clearly, water undergoes surface dynamic surface exchange and hydrolysis reactions at the surface. On the other hand, ethanol has a substantially lower dielectric constant (ε = 24.3) than H_2O (ε = 80.4). As a consequence, we predict that the relative thickness of the electrical double layer should decrease over the mole fraction range of χ_{EtOH} from 0 to 1. The thickness of the electrical double layer

around the CdS particles, which under the conditions of our experiments is negatively charged, can be determined as follows[107]:

$$\kappa \equiv \left(\frac{2\,F^2 \mu}{\varepsilon \varepsilon_0 RT} \right)^{0.5} \tag{5.27}$$

where ε is the dielectric constant of the solvent or mixed solvent system, ε_0 is the permittivity of free space (8.854×10^{-12} C^2 J^{-1} m^{-1}), μ is the ionic strength of the background electrolyte (mol m^{-3}), R is the gas constant (8.314 J mol^{-1} K^{-1}), T is temperature in units of K, and F is the Faraday constant (96485 C mol^{-1}). With ε = 78.5 (X_{EtOH} = 0) and ε = 24.3 (X_{EtOH} = 1), the thickness of the electrical double layer for an ionic strength of 1.0 mol m^{-3} at T = 298 K gives $\kappa_{H_2O}^{-1} = 9.6\,\text{nm}$ and $\kappa_{EtOH}^{-1} = 5.4\,\text{nm}$, respectively. Double layer compression in the presence of an increasing mole fraction of ethanol will impact the fluorescence response by enhancing the physicochemical interaction of ethanol with the charged CdS surface and thus increasing the fluorescence intensity. In addition, the surface-bound or near surface ethanol serves as a more effective hole trap. Therefore, the apparent exponential increase in fluorescence intensity is due to a more efficient hole trapping by ethanol, which is enhanced because of the compression of the electrical double layer at the same ionic strength (i.e., the effective concentration of ethanol at the surface is increased).

The dramatic color change from yellow to gray during photolysis and H_2 generation suggests that the traditional mechanistic view of proton reduction or hydrogen generation in the presence of alternative electron donors should be revised. The observed color change is due to the rapid photoreduction of Cd(II) to Cd(I) and then to Cd(0) on the surface of CdS in the absence of oxygen. There is also some probability that S(-II) in the

CdS matrix is also oxidized partially by trapped valence band holes to form S(0) and eventually polysulfide ion (S_2^{2-}). Upon exposure to oxygen, the yellow color is regenerated over several hours with the return of yellow CdS on the nanocomposite structures.

The photoreduction of metal sulfides upon exposure to UV or visible radiation is well documented [108-120]. For example, Stroyuk et al. [121] reported that added Cd^{2+} adsorbed on the surface of CdS was reduced to Cd(0) upon illumination with visible light, while Job and Ernschwiller [122] noted that ZnS was photoreduced to Zn(0) while S(-II) was oxidized to elemental sulfur, S(0). They[122] also noted that H_2 was liberated via the reaction Zn(0) + 2 $H^+ \rightarrow H_2 + Zn^{2+}$. In addition, enhanced photochemical activities have been reported after photoreduction of metal sulfides [110,111,123].

Gutierrez and Henglein [124] reported that highly reactive elemental Cd deposits were formed during the illumination of colloidal CdS is illuminated in the presence of SO_3^{2-} or $S_2O_4^{2-}$. They reported quantum yields for the formation of Cd(0) of $\phi = 0.005$ in the absence of excess Cd^{2+} and $\phi = 0.053$. They also noted that H_2 was produced after the formation of Cd(0) on the CdS surface. They argued that hydrogen formation was dependent on a large overpotential for the reduction of water by excess electrons in CdS and the catalytic action of a surface Cd(0) layer. Gutierrez and Henglein[124] also reported that Cd(0) was formed with at close to 100% efficiency when colloidal CdS was irradiated with γ-rays in the presence of organic electron donors.

In our experiments and those of Gutierrez and Henglein[124], H_2 production is preceded by the initial photoreduction of CdS. A probable set of surface chemical reactions that include photoreduction are as follows:

$$\overset{S^{2-}}{\underset{Cd^{2+}}{}}>Cd(+II)S(-II)H_2^+ \xrightarrow{h\nu} \xrightarrow[h_{vb}^+]{\bar{e}_{cb}} \overset{S^{2-}}{\underset{Cd^{2+}}{}}>Cd(+I)S(-I)H_2^+ \quad (5.28)$$

$$\overset{S^{2-}}{\underset{Cd^{2+}}{}}>Cd(+I)S(-I)H_2^+ \xrightarrow{h\nu} \xrightarrow[h_{vb}^+]{\bar{e}_{cb}} \overset{S^{2-}}{\underset{Cd^{2+}}{}}>Cd(0)S(0)H_2^+ \quad (5.29)$$

$$\overset{S^{2-}}{\underset{Cd^{2+}}{}}>Cd(0)S(0)H_2^+ \rightleftharpoons \overset{S^{2-}}{\underset{Cd^{2+}}{}}>Cd(+II)S(0)^+ + H_2 \quad (5.30)$$

$$\overset{S^{2-}}{\underset{Cd^{2+}}{}}>Cd(+II)S(0)^+ + CH_3CH_2OH \rightleftharpoons \overset{S^{2-}}{\underset{Cd^{2+}}{}}>Cd(+II)S(-I)H^+ + CH_3\dot{C}HOH \quad (5.31)$$

$$\overset{S^{2-}}{\underset{Cd^{2+}}{}}>Cd(+II)S(-I)H^+ + CH_3CH_2OH \rightleftharpoons \overset{S^{2-}}{\underset{Cd^{2+}}{}}>Cd(+II)S(-II)H_2^+ + CH_3\dot{C}HOH \quad (5.32)$$

$$2\,H^{\cdot} \longrightarrow H_2 \quad (5.33)$$

$$2\,CH_3\dot{C}HOH \longrightarrow 2\,CH_3CHO + H_2 \quad (5.34)$$

Similar photoreactions can occur at neutral >CdSH and >CdOH sites and protonated surface sites involving $>CdSH_2^+$ and $>CdOH_2^+$.

$$\overset{S^{2-}}{\underset{Cd^{2+}}{}}>Cd(+II)S(-II)H \xrightarrow{h\nu} \xrightarrow[h_{vb}^+]{\bar{e}_{cb}} \overset{S^{2-}}{\underset{Cd^{2+}}{}}>Cd(+I)S(-I)H \quad (5.35)$$

$$\overset{S^{2-}}{\underset{Cd^{2+}}{}}>Cd(+I)S(-I)H \xrightarrow{h\nu} \xrightarrow[h_{vb}^+]{\bar{e}_{cb}} \overset{S^{2-}}{\underset{Cd^{2+}}{}}>Cd(0)S(0)H \quad (5.36)$$

$$\overset{S^{2-}}{\underset{Cd^{2+}}{}}>CdOH_2^+ \xrightarrow{2\,\bar{e}_{cb}} \overset{S^{2-}}{\underset{Cd^{2+}}{}}>CdO^- + H_2 \quad (5.37)$$

$$\overset{S^{2-}}{\underset{Cd^{2+}}{}}>CdO^- + 2H^+ \xrightarrow{2\,\bar{e}_{cb}} \overset{S^{2-}}{\underset{Cd^{2+}}{}}>CdOH_2^+ \quad (5.38)$$

$$\overset{S^{2-}}{\underset{Cd^{2+}}{}}>CdOH \xrightarrow{h_{vb}^+} \overset{S^{2-}}{\underset{Cd^{2+}}{}}>CdOH^{+\cdot} \xrightarrow{CH_3CH_2OH} \overset{S^{2-}}{\underset{Cd^{2+}}{}}>CdOH_2^+ + CH_3\dot{C}HOH \quad (5.39)$$

The increase in H_2 production with an increase in pH suggests that the >CdOH surface site may play an important role in the initial steps of proton reduction (a proton bound to O^{2-}) on the surface of CdS.

$$\overset{S^{2-}}{\underset{Cd^{2+}}{}}>CdOH + \bar{e}_{cb} \longrightarrow \overset{S^{2-}}{\underset{Cd^{2+}}{}}>CdO^- + H^{\cdot} \quad (5.40)$$

Shiragami et al.[125] reported that CdS suspensions photolyzed in the presence of CH_3OH turn brown due to the internal reduction of lattice Cd(+II) to Cd(0). In addition, they estimated the amount of Cd(0) produced using the method of Gutierrez and Henglein[124]. They also reported 1) that the brown colored colloidal suspension gave an absorption spectrum that was red-shifted ($\lambda_{abs} > 600$ nm), and 2) that the yellow color was restored upon the reintroduction of oxygen into the system as we observed in our experiments.

Reber and Meier[126] reported that ZnS is photoreduced to form metallic zinc clusters on the surface of ZnS as follows:

$$Zn(II)S(-II) \xrightarrow{2\,h\nu} Zn(0) + S(0) \tag{5.41}$$

When methanol was used as an electron donor the following dehydrogenation was observed [126]:

$$Zn(II)S(-II) + CH_3OH \xrightarrow{2\,h\nu} Zn(0) + H_2 + HCHO \tag{5.42}$$

They concluded that the high observed photoreactivity for H_2 production ($\phi_{H_2} = 0.9$ at $\lambda_{max} = 313$ for $E_g = 3.66$ eV) was due primarily to the formation of elemental zinc clusters on the surface, and that the Zn(0) clusters served as electron transfer catalysts.

In a later study, Ohtani and co-workers[127] examined the photolysis of an of 2,6-diaminopimelic acid in an anoxic suspension of heat-treated, bulk-phase CdS. They argued that the heat-treated CdS resulted in sulfur vacancies which contributed to the formation of Cd(0) on the surface.

Since the formation of Cd(0) on the surface appears to precede the production of H_2, can use a simple steady-state analysis[125] to predict the kinetics of the photoreduction. The production of Cd(0) after excitation to produce electrons, e^-_{cb}, and holes, h^+_{vb}, and on

the surface of CdS can be written as follows:

$$\frac{d[Cd(0)]_{surf}}{dt} = k_{red}[Cd(II)]_{surf}[e^-_{cb}]^2 \quad (5.43)$$

$$\frac{d[e^-_{cb}]}{dt} = \alpha I_0 - k_{rc}[e^-_{cb}][h^+_{vb}] - k_{red}[e^-_{cb}][Cd(II)]_{surf} - k_{tr}[e^-_{cb}][\cdot CH_2CH_2OH] - k_1[e^-_{cb}][H^+]_{surf} - k_2[e^-_{cb}][H\cdot]_{surf} \quad (5.44)$$

$$\frac{d[h^+_{vb}]}{dt} = \alpha I_0 - k_{rc}[e^-_{cb}][h^+_{vb}] - k_3[CH_3CH_2OH]_{surf} \quad (5.45)$$

If we assume steady-state conditions for eqs. 5.43–5.45, we obtain

$$\left[e^-_{cb}\right]_{ss} = \frac{\alpha I_0}{\left(k_{red}[Cd(II)]_{surf} + k_{tr}[\cdot CH_2CH_2OH]_{surf}\right)} \quad (5.46)$$

$$\left[h^+_{vb}\right]_{ss} = \frac{\alpha I_0}{\left(k_3[CH_3CH_2OH]_{surf}\right)} \quad (5.47)$$

$$\left[\cdot CH_2CH_2OH\right]_{ss} = \frac{\left(k_3[CH_3CH_2OH]_{surf} - k_{red}[Cd(II)]_{surf}\right)}{\left(k_{rc}\right)} = \beta \quad (5.48)$$

With eqs. 5.46–5.48, we can recast eq. 5.43 as follows:

$$\frac{d[Cd(0)]_{surf}}{dt} = \frac{\alpha I_0^2 k_{red}[Cd(II)]_{surf}}{\left(k_{red}[Cd(II)]_{surf} + k_{tr}\beta\right)^2} = \gamma I^2_{abs} \quad (5.49)$$

where $I_{abs} = \alpha I_0^2$ and $\alpha k_{red}[Cd(II)]_{surf} \Big/ \left(k_{red}[Cd(II)]_{surf} + k_{tr}\beta\right)^2 = \gamma$. Equation 49 shows that the rate of production of elemental cadmium on the surface of CdS depends on the absorbed light intensity squared (i.e., $I_{abs} = \alpha I_0$).

Colloidal Cd(0) has been shown to mediate H_2 formation in the presence of organic radicals. For example, colloidal Cd(0) particles are able to produce H_2 from 1-hydroxy-1-methylethyl radicals as follows[128]:

$$2\,(CH_3)_2\dot{C}OH \xrightarrow{Cd(0)} 2\,(CH_3)_2CO + H_2 \quad (5.50)$$

Resch et al.[73] observed a strong dependence of the fluorescence behavior of stabilized CdS colloids in which the most intense fluorescence is obtained with solvent with the lowest dielectric constants. These results coupled with our own observations, allows us to conclude that the alcohols have a dual purpose. They serve primarily as sacrificial electron donors but also allow stronger interactions of protons with charged CdS or zeolite surfaces by decreasing the dimensions of the charge field or the electric double layer. In effect, the closer bonding interaction with the surface of CdS and Cd(0) resulted in more favorable conditions for electron transfer to surface-bound protons and subsequently for the production of molecular oxygen.

Since the early work of Herron and co-workers [70-72,76] on CdS-Zeolite composites, there have been a number of investigations of the photocatalytic properties of CdS encapsulated in zeolite cavities. Most often the enhanced reactivity has been attributed to enhanced electron-hole charge separation and the increased stability[70] of the CdS has been explained in terms of stabilization of oxygen atoms in the zeolite cages.

Guan and co-workers[129] reported that CdS formed in zeolite-ETS-4 and titanium silicate loaded ETS-4 were effective catalysts for H_2 production at $\lambda > 420$ nm in the presence of HS^- and SO_3^{2-} as sacrificial electron donors at pH 14 (i.e., 1.0 M NaOH), and that the CdS embedded in the ETS-4 cavities was resistant to photocorrosion. Furthermore, nanoparticulate CdS in the ETS-4-Zeolite showed enhanced activity relative to naked CdS suspensions. The enhanced activity is often explained in terms of the injection of conduction band electrons into the lower-lying bands of the host material. This is consistent with the observed blue shifts (Figure 5.4) which were noted in the fluorescence spectra that are attributed to ‘quantum confinement’ within zeolite cages.

The order of photocatalytic activity for the potassium niobate composites with respect to H_2 production is Ni(0)/NiO/$KNbO_3$/CdS > Ni(0)/$KNbO_3$/CdS > $KNbO_3$/CdS under identical reaction conditions. The $KNbO_3$ backbone of the composite has unusual chemical and physical material properties. Potassium niobate crystals are used in in optical waveguides, in nonlinear optical devices (e.g., frequency doubling and wavelength mixing), in piezoelectric devices (e.g., tunable frequency ultrasound transducers), in holographic image storage, and as a wide-band gap photocatalyst (ΔE_g = 3.4 eV).

Hayashi et al. [130] synthesized $KNbO_3$ hydrothermally and found that the fine crystalline powders were efficient photocatalysts for the production of H_2 under UV light illumination at 254 nm. Under slightly different synthesis conditions, they produced $K_4Nb_6O_{17}$ which was found to be substantially less active than $KNbO_3$ for H_2 production. They also provided ESR evidence for photoreduction of ion-exchanged Ni^{2+} on $KNbO_3$ to form Ni(0) in the presence of methanol. In addition, Hayashi et al. found that hydrothermally produced $KNbO_3$ was more photoreactive than potassium niobate ($K_4Nb_6O_{17}$) synthesized by the solid-state reaction at 1130 ^oC. Moreover, high H_2 production rates and actual photosplitting of water to form O_2 also required Ni(0) formation on the surface.

Other unique properties[131] of $KNbO_3$ that may explain its cooperative effects in the Ni(0)/NiO/$KNbO_3$/CdS. For example, Ewart et al.[131] reported that mobile electrons are generated in electrochemically reduced and Fe-doped $KNbO_3$ upon excitation at 532 nm. The electrons photoexcited at 532 nm had lifetimes of 4 ns and electron mobility of 0.5 $cm^2\ V^{-1}\ s^{-1}$. They conclude that the photoexcited electrons are trapped within 4 ns (i.e.,

loss of detectable mobility), however, the trapped-state electrons are thermally activated on a millisecond timeframe and eventually recombine with the internal donor states.

In the case of $KNbO_3$ produced by our synthetic procedure, we thermally treated the pure $KNbO_3$ powders at 500 ^oC in an H_2 atmosphere. This treatment step may lead to creation of oxygen vacancies or formation of Nb(IV) and Nb(III) states. After reduction with H_2 the white $KNbO_3$ samples are converted into a gray material which seems to indicate Nb(V) reduction has taken place. Kesselman et al.[132] had observed a similar reduction in Nb_2O_5/TiO_2 composites that were reduced over hydrogen at high temperatures.

A portion of the enhanced reactivity in the $KNbO_3$ composites may be due to involvement of the reduced states of niobium and/or oxygen vacancies that allow for the photoexcitation of mobile electrons with visible light. The longer lifetimes (τ_{tr} > ms) of the trapped electrons may contribute to the higher reduction rates for bound protons or hydroxides. Reduction of Nb_2O_5 is known to form a variety of phases such as $Nb_{12}O_{29}$, $Nb_{22}O_{54}$, $Nb_{25}O_{62}$, and $Nb_{47}O_{116}$ that involve partial oxygen loss coupled with the formation of Nb(IV). Similar mixed valence state phases should coexist within the framework of reduced $KNbO_3$ and contribute to the photoexcitation of electrons and to the overall photoreactivity with visible light.

Another relevant feature of the metal niobates[133](e.g., $LiNbO_3$ and $KNbO_3$) for electro-optic and photorefractive applications is the activation of surface protons (i.e., protons bound in hydroxyl ions, ^-OH). The hydroxyl bound protons have activation energies in the range of 1 ev for mobility in $KNbO_3$ crystals.

In order to understand the complex interactions taking place on

Ni(0)/NiO/$KNbO_3$/CdS we need to account for the impact of the NiO coated Ni deposits on the surface of $KNbO_3$. It is generally understood that Ni serves of collect conduction band electrons similar to Pt deposits on semiconducting surfaces. The NiO surface mostly likely reacts in similar fashion as in the case of the >NbOH surface groups. The pH_{zpc} of NiO ranges from 7.5 to 7.9. Thus, the catalytic effect of combined Ni/NiO deposits may be due to the following sequence involving surface hydroxyl groups on the hydrated NiO surface:

$$Ni^{o} : \bar{e}_{m} + > NiOH \longrightarrow > NiO^{-} + H^{\cdot} \quad (5.57)$$

In this pathway, the mobile electrons from both photoactivated CdS and $KNbO_3$ are captured by the NiO and transferred to the >NiOH surface groups for formed hydrogen atoms and eventually molecular hydrogen.

In conclusion, we note that the Ni/NiO/$KNbO_3$/CdS composite after photoreduction has some of the components that comprise a Ni-Cd battery. At pH 14, the redox chemistry of a Ni-Cd battery is as follows:

$$Cd^{0} + 2\,^{-}OH \longrightarrow Cd(OH)_2 + 2\,\bar{e} \quad (E_b^0 = 0.81\ V) \quad (5.58)$$

$$NiO_2 + H_2O + 2\,\bar{e} \longrightarrow Ni(OH)_2 + 2\,^{-}OH \quad (E_b^0 = 0.49\ V) \quad (5.59)$$

$$NiOOH + H_2O + 1\,\bar{e} \longrightarrow Ni(OH)_2 + {}^{-}OH \quad (E_b^0 = 0.59\ V) \quad (5.60)$$

$$2\,NiOOH + 2\,H_2O + Cd^{0} \longrightarrow Ni(OH)_2 + Cd(OH)_2 \quad (E_{rxn}^{b} = 1.40\ V) \quad (5.61)$$

During recharging of a Ni-Cd battery with a sufficient over-potential, H_2 is evolved. The bandgap energy of NiO is 3.5 eV [134], and thus, it should not be photoactive in our experiments. However, given the redox potential of eq. 5.62, it may be possible to run the reaction with light < 900 nm. At 500 nm (i.e., 2.48 eV), a sufficient over-potential could be achieved to generate H_2.

$$H_2O + Cd^0 \longrightarrow CdO + H_2 \quad (E^0_{rxn} = -0.087\ V) \tag{5.62}$$

Acknowledgements

We are grateful to the Hydrogen Energy R&D Center of the 21st Century Frontier Research and Development Program of the Ministry of Science and Technology of Korea for financial support. Additional support was provided graciously by the Fellowship Program of the Korean Science & Engineering Foundation (KOSEF) and the Davidow Research Fund of the California Institute of Technology.

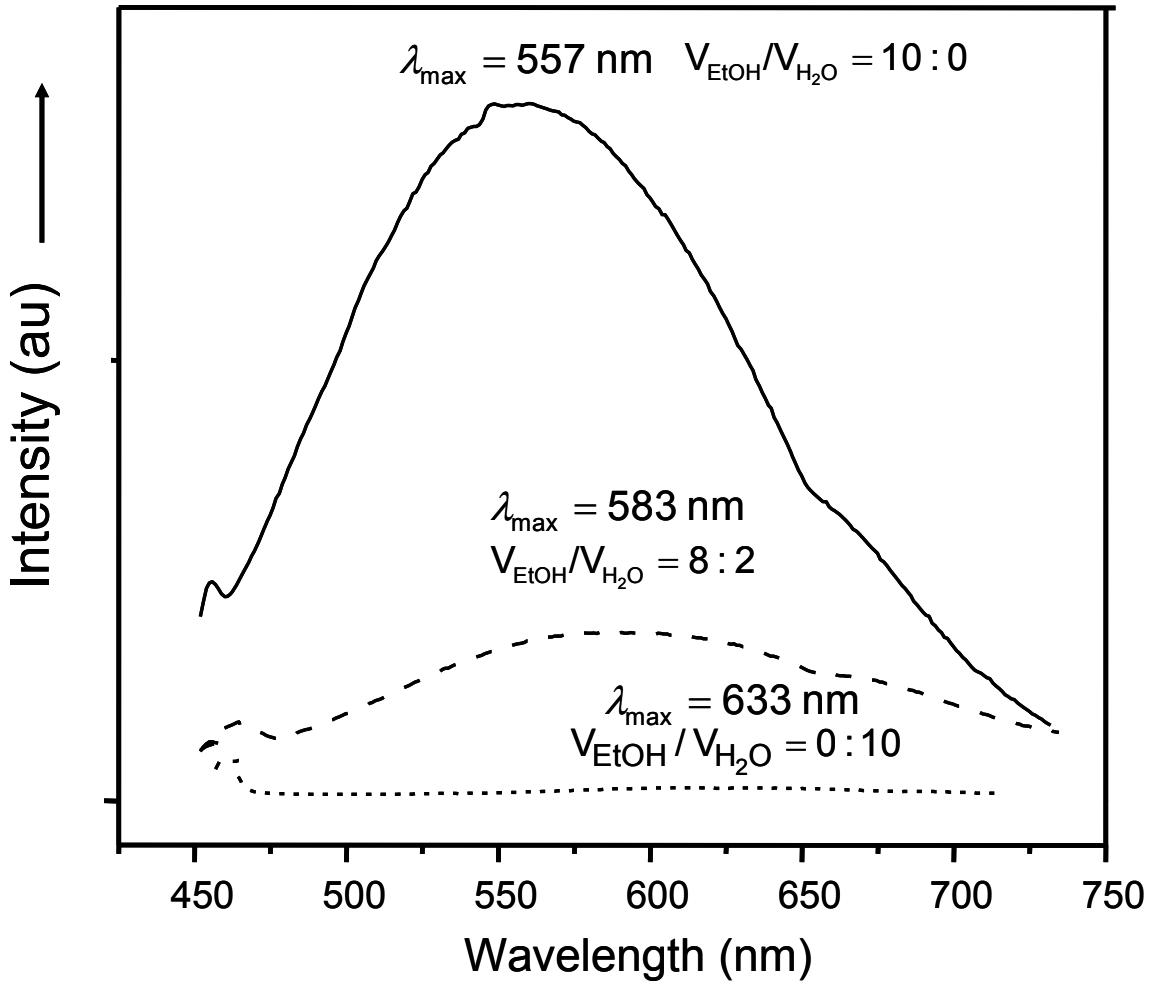

Figure 5.1. Fluorescence emission spectra of CdS colloids (5.0×10^{-4} M) a function of the ethanol-water volume ratio, V_{EtOH}/V_{H_2O}. The highest intensity is obtained in neat ethanol with a small amount (≈ 1.0 mM) H_2O present as a trace contaminant. V_{EtOH}/V_{H_2O} = 0:10 represents pure water and V_{EtOH}/V_{H_2O} = 10:0 is 99.99% ethanol.

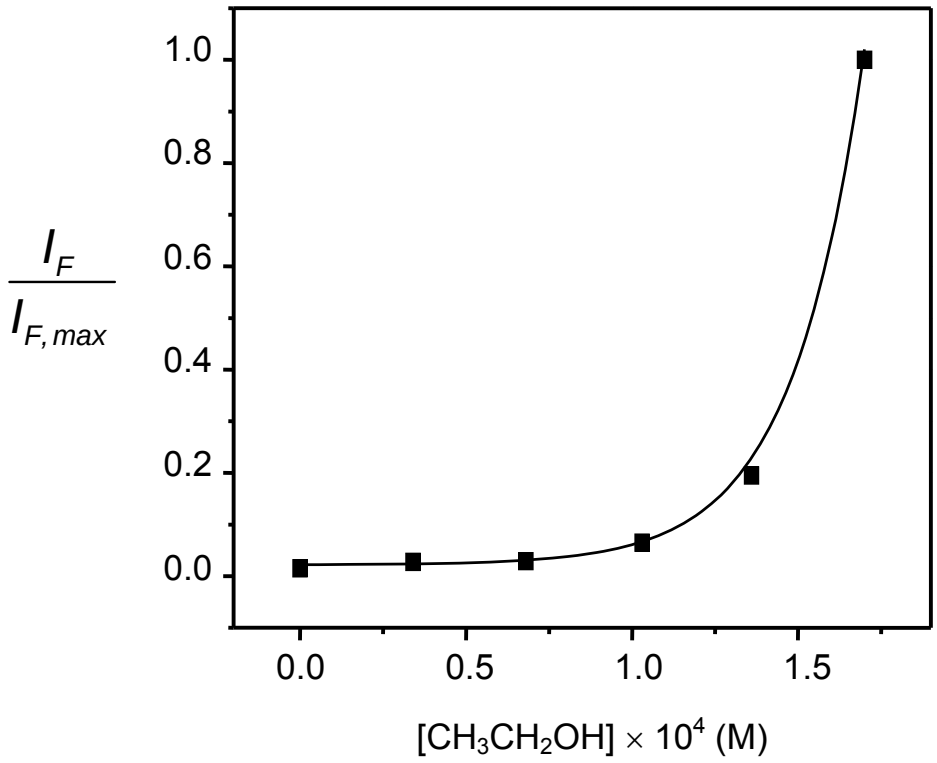

Figure 5.2. Fluorescence emission intensity of CdS colloids as a function of $[CH_3CH_2OH]$ in H_2O at 25 ^oC

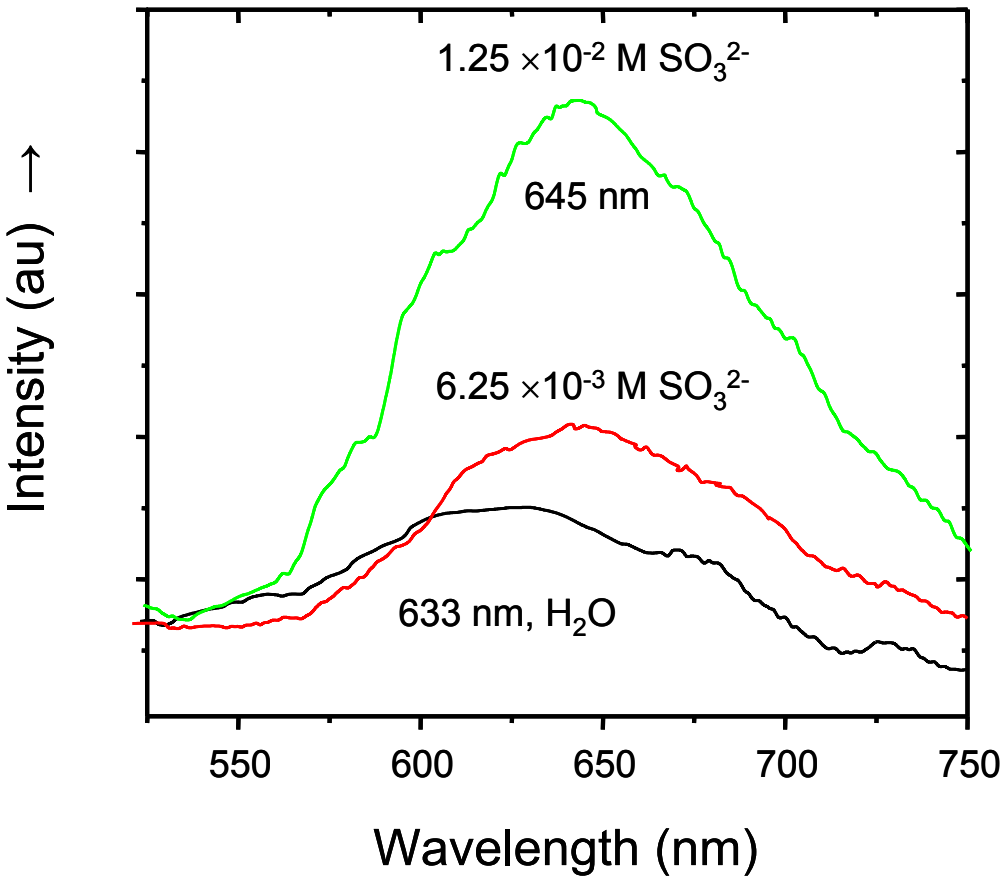

Figure 5.3. Fluorescence emission spectra of CdS colloids (5.0×10^{-4} M) vs. [SO_3^{2-}] at pH 8. (a) H_2O, (b) 6.25×10^{-3} M K_2SO_3, and (c) 1.25×10^{-2} M K_2SO_3

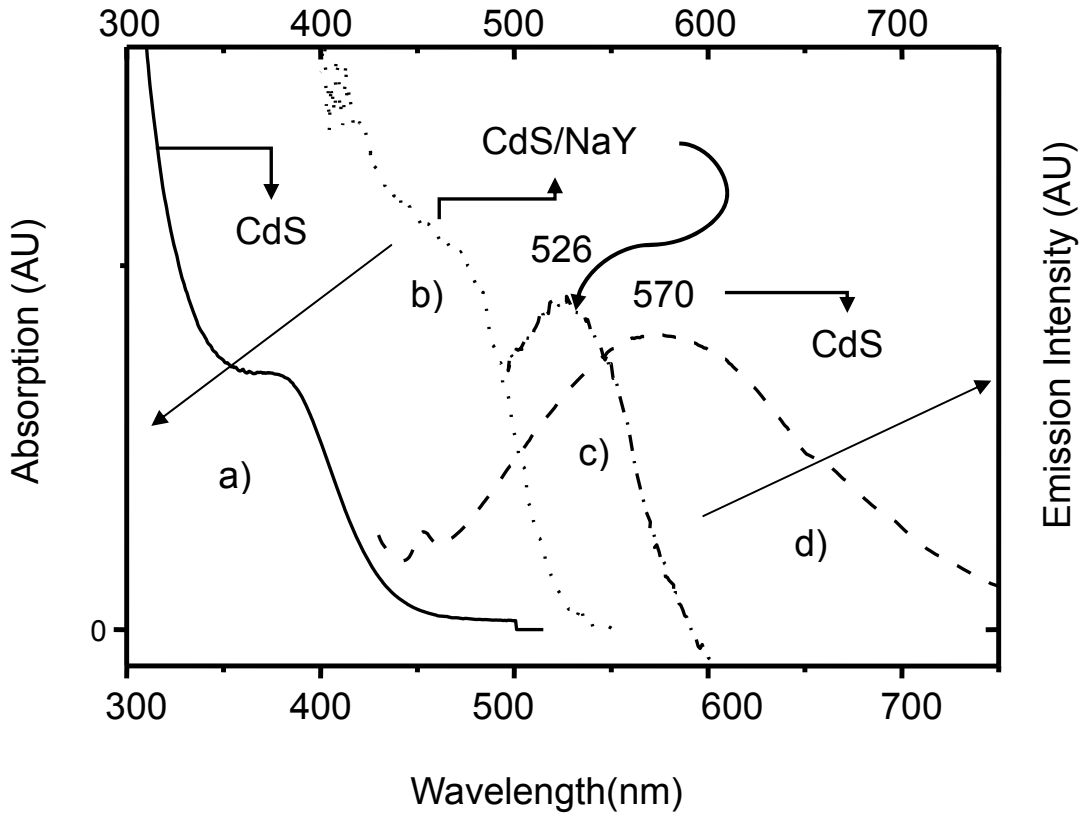

Figure 5.4. Diffuse reflectance and fluorescence emission spectra of CdS embedded in NaY zeolite as compared to naked Q-size CdS colloids in EtOH. a) absorption of the CdS colloids in EtOH, b) absorption of CdS/NaY zeolite, c) emission of CdS/NaY zeolite, and d) emission of the CdS colloids in EtOH

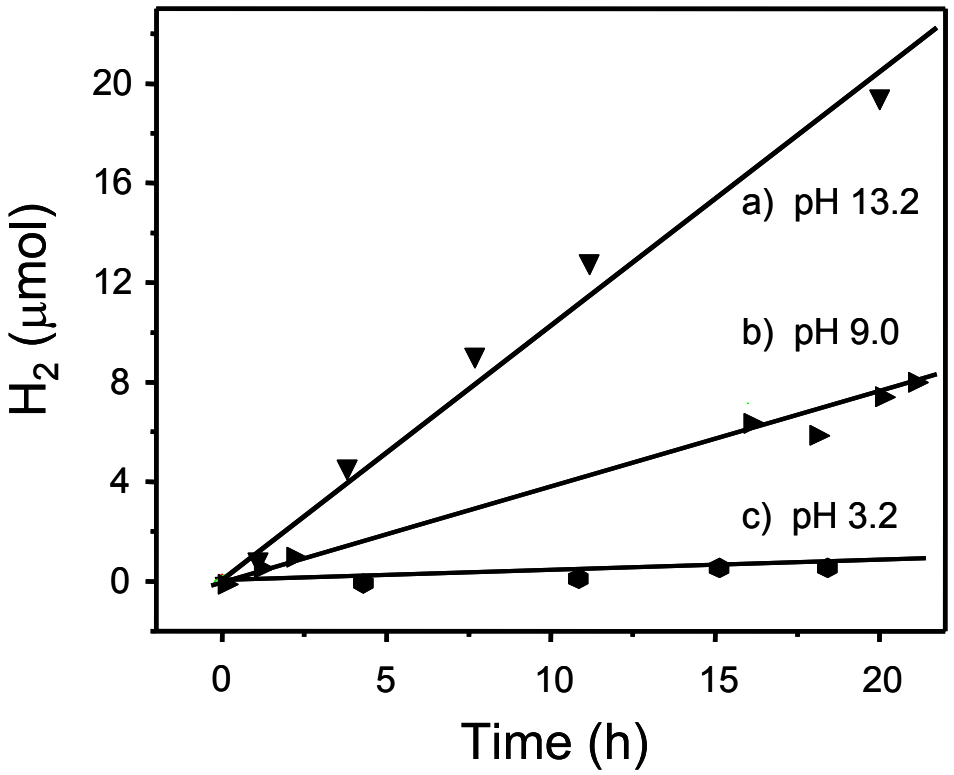

Figure 5.5. H_2 production rates on nanoparticulate CdS colloids at [CdS] = 5.0×10^{-4} M) in EtOH:H_2O = 1:1 mixtures. V_T = 40 mL). a) [NaOH] = 0.1 M, pH 13.2; b) [K_2SO_3] = 5.0×10^{-3} M and [$Cd(OOCCH_3)_2$] = 5.0×10^{-4} M) pH 9; c) [K_2SO_3] = 5.0×10^{-4} M and [CH_3CO_2H] = 0.1 M, pH 3.2.

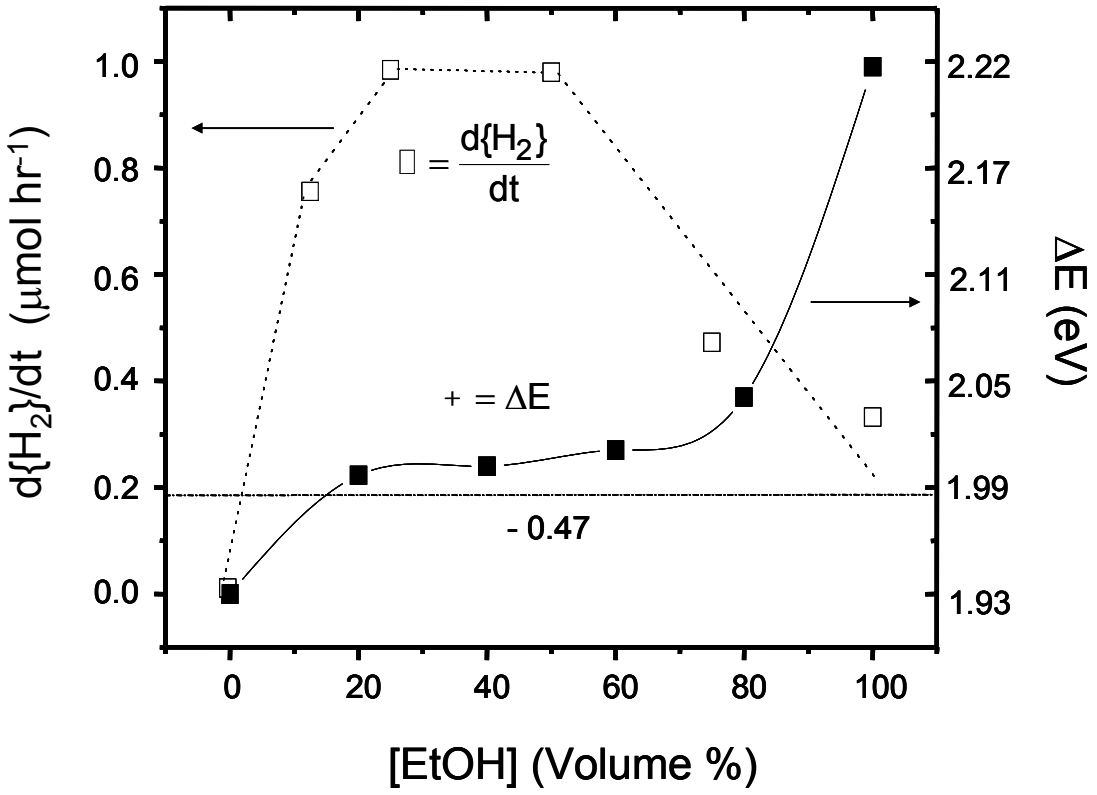

Figure 5.6. A plot of the energy gap, ΔE (eV), between the emissive state and the ground state calculated from the fluorescence emission spectra as a function of ethanol volume ratio in water. The squares show the rate of H_2 evolution as a function of V_{EtOH} / V_{H2O} calculated from the slopes of linear reaction progress plots for the photolysis condition given in Figure 5. The dashed line (-·-·-) denotes the relative energy position for $2\ H^+ + 2\ \bar{e} \rightarrow H_2$ at pH 8.

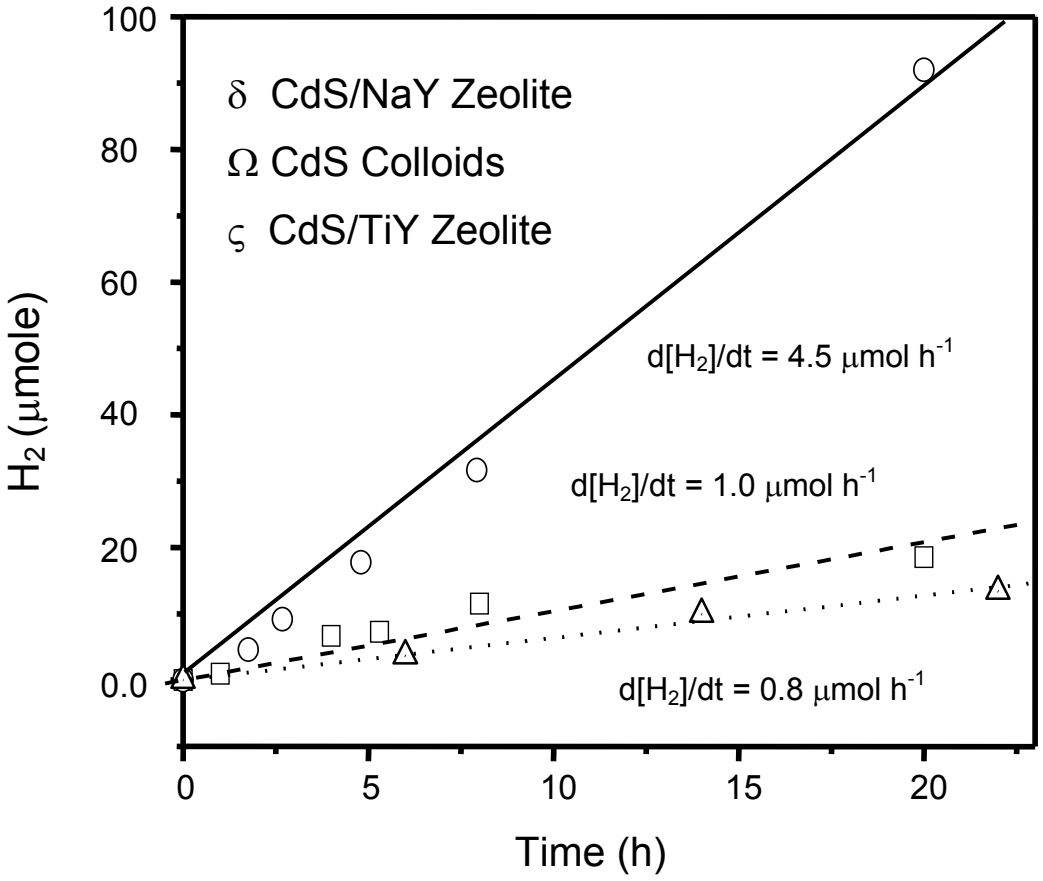

Figure 5.7. Rates of H_2 evolution in a mixed ethanol water solvent (EtOH:H_2O = 1:3 V/V) for V_T = 40 mL with visible light irradiation (λ > 400 nm) versus time. Data presented for CdS colloids, □, ([CdS] = 2.5×10^{-4} M), for CdS/NaY zeolite, ○, ([CdS/NaY] = 0.2 g in 40 mL at 2.9 wt% CdS), and for CdS/TiY zeolite, Δ, ([CdS/TiY] = 0.2 g in 40 mL at 2.9 wt% CdS)

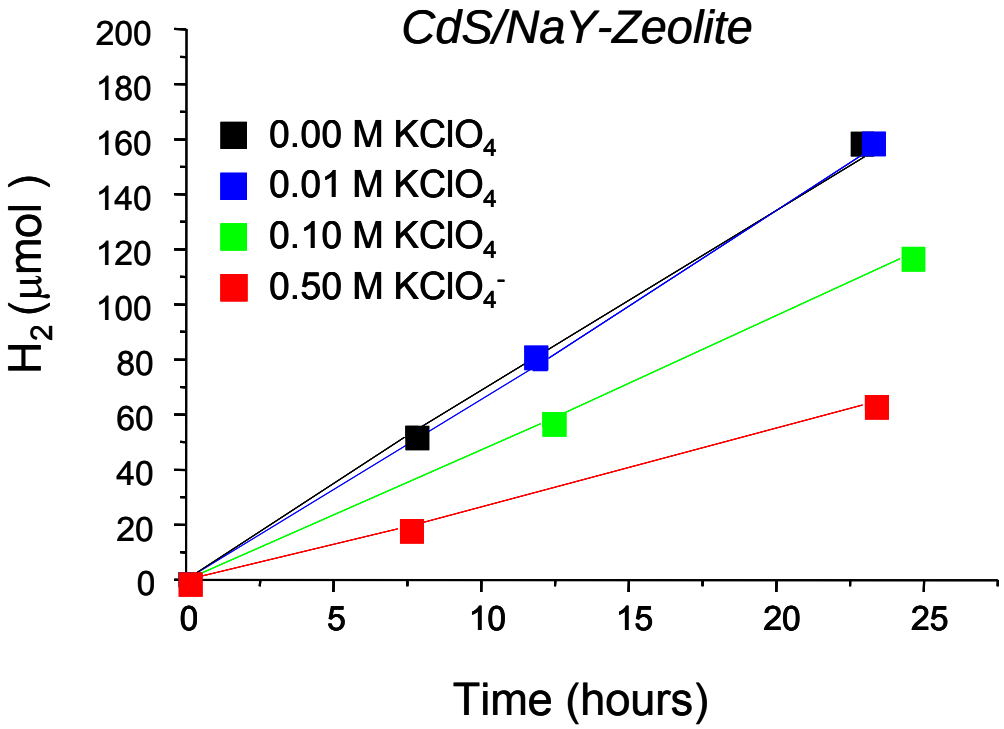

Figure 5.8. Rates of H_2 evolution in a mixed ethanol water solvent (EtOH:H_2O = 1:3 V/V) for V_T = 40 mL as a function of ionic strength with visible light irradiation ($\lambda > 400$ nm) using the NaY-Zeolite/CdS composite

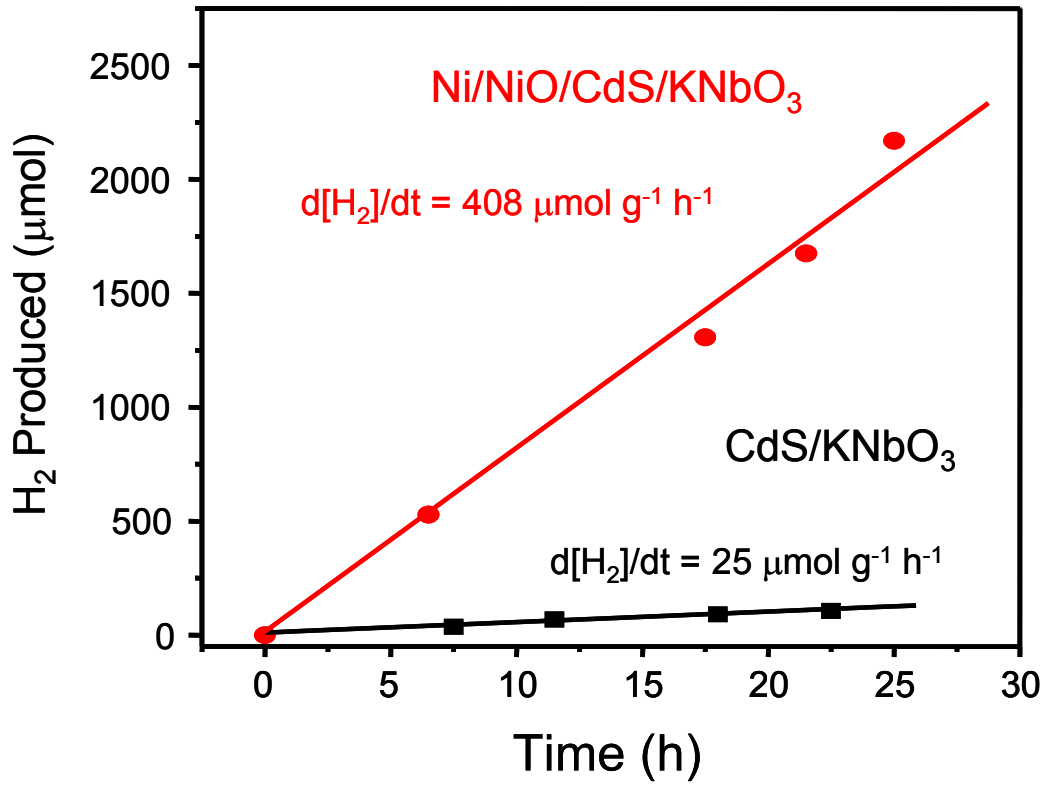

Figure 5.9. Rate of H_2 evolution under visible light irradiation ($\lambda > 400$ nm) in a mixed ethanol water solvent (EtOH:H_2O = 1:3 V/V, V_T = 40 mL) for the Ni/NiO/$KNbO_3$/CdS nanocomposite

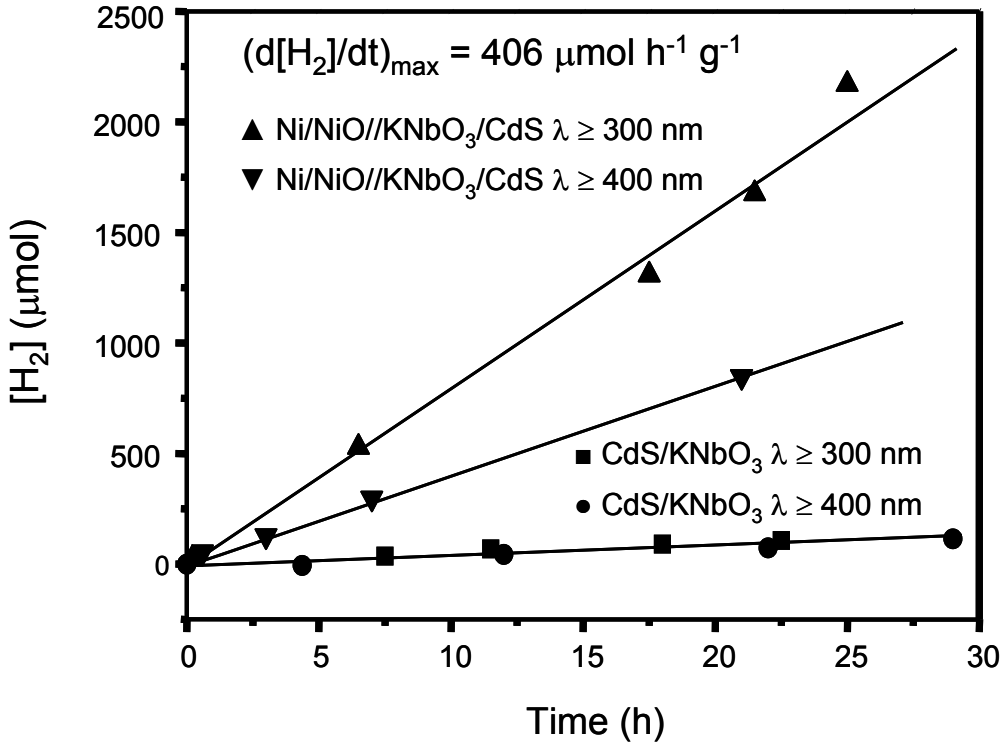

Figure 5.10. Comparison of the rate of H_2 evolution under visible light irradiation (λ > 400 nm) compared to UV-vis light (λ > 300 nm) in a mixed ethanol water solvent (EtOH:H_2O = 1:3 V/V, V_T = 40 mL) for the Ni/NiO/$KNbO_3$/CdS nanocomposite

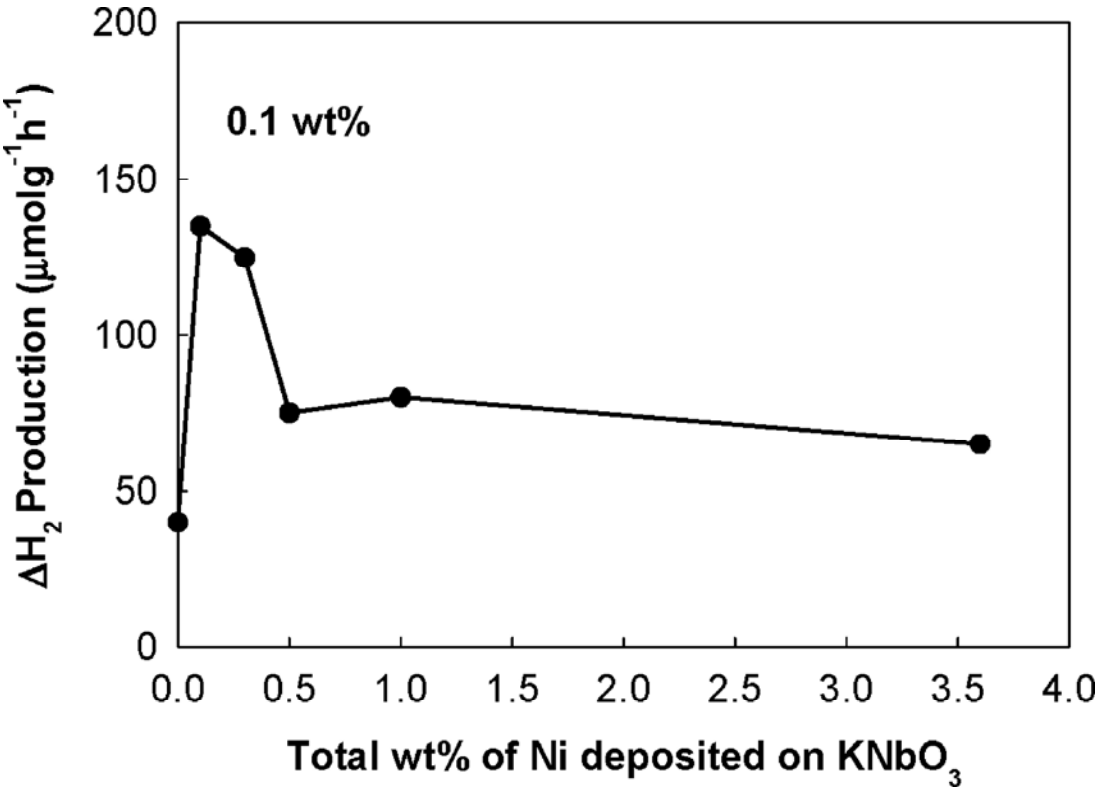

Figure 5.11. Differential rate (μmol h^{-1}) of H_2 production on Ni(0)/NiO/$KNbO_3$/CdS as a function of the weight percent Ni deposition. The optimal is approximately 0.1 wt%. [nanocomposite] = 0.2 g L^{-1}, V_T = 50 mL^{-1}. Saturated with Ar at t = 0. Samples irradiated with a 500 W Xenon lamp at $\lambda \geq 400$ nm

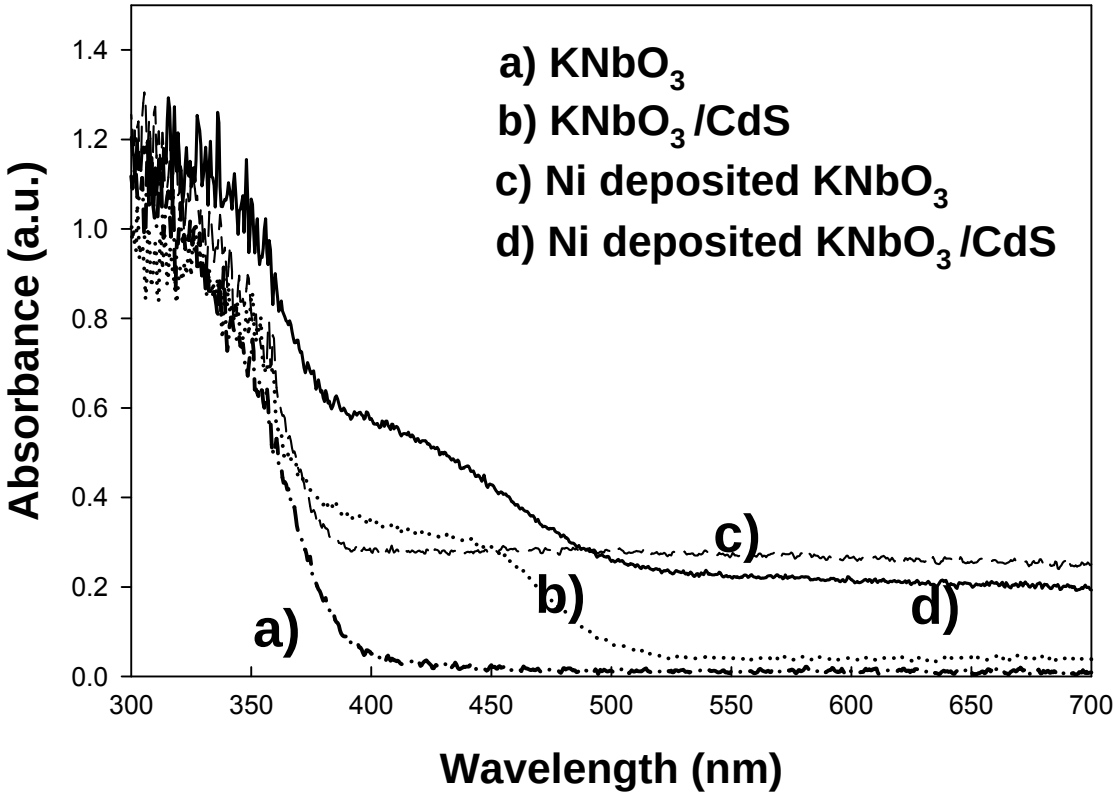

Figure 5.12. UV-vis spectra for a) $KNbO_3$, b) $KNbO_3$/CdS, c) 0.1 wt% Ni(0)/NiO/ $KNbO_3$, and d) 0.1 wt% Ni(0)/NiO/$KNbO_3$/CdS

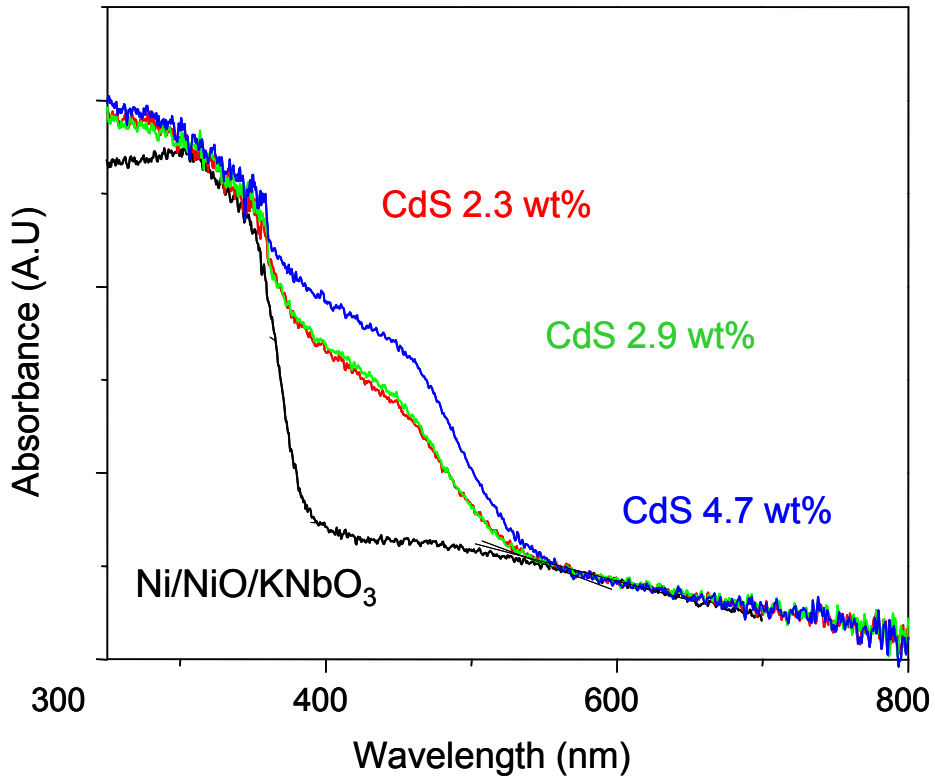

Figure 5.13. UV-vis spectra for Ni/NiO/$KNbO_3$/CdS as a function of the wt% loading of Q-CdS

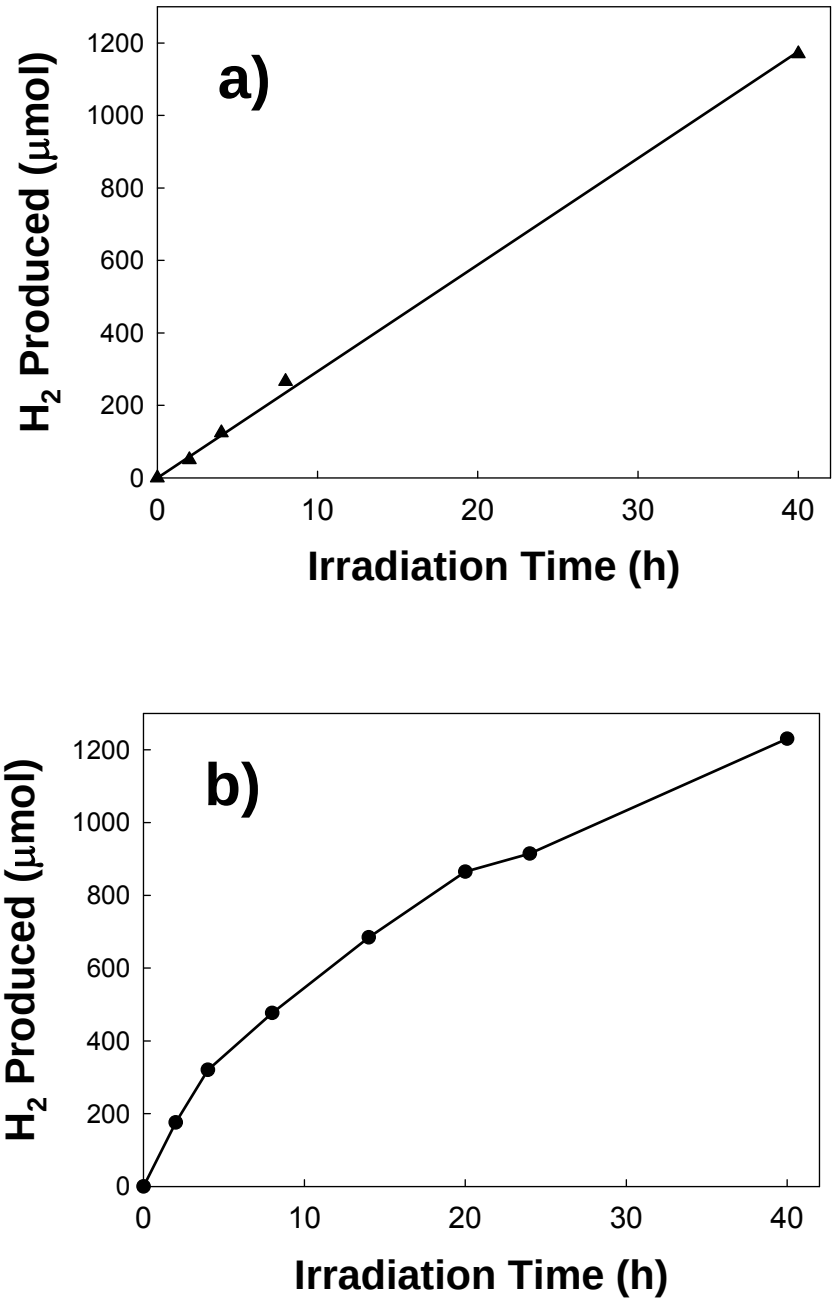

Figure 5.14. Hydrogen production on nanocomposite $KNbO_3$/CdS in an isopropanol/ water solvent mixture (1:3). a) Ni(0) and NiO deposits on the surface of $KNbO_3$/CdS. b) Ni(0) deposits only on the surface of $KNbO_3$/CdS. 0.1 wt% Ni as Ni(0) or Ni(0)/NiO on CdS/$KNbO_3$ samples. [nanocomposite] = 0.2 g, V_T = 50 mL.

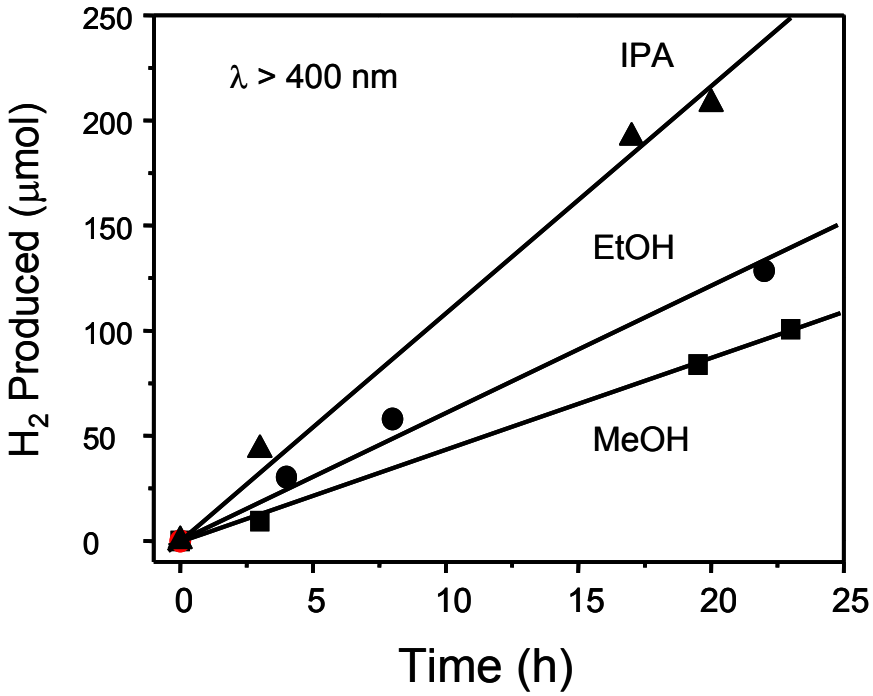

Figure 5.15. Relative rates of H_2 production as a function of the electron donor (ROH) on $KNbO_3$/CdS

TABLE 5.1. H_2 evolution rates of Q-CdS /$KNbO_3$ nanocomposites

Sample	Band-gap/eV	Incident light/nm	H_2 evolution rate(μmole/g-h)	Q.Y
$KNbO_3$	3.26	>300 nm	*No*	
$NiKNbO_3$	3.15	>300 nm	< 1	
$CdS/KNbO_3$	2.65	>300 nm	25	
$CdS/KNbO_3$	2.65	>400 nm	20	
$CdS/Ni(0.1\%)KNbO_3$	2.38	>300 nm	408	
$CdS/Ni(0.1\%)KNbO_3$	2.38	>400 nm	203.5	8.8 %
$CdS/Pt(0.1\%)KNbO_3$	2.46	>400 nm	147	

* The amount of CdS is 5 X 10^{-4} mole/g, solvent: IPA:H_2O (1:3 (v/v))

References

(1) Bard, A. J. *Journal of Photochemistry* **1979**, *10*, 59.

(2) Sakata, T.; Kawai, T. *Chemical Physics Letters* **1981**, *80*, 341.

(3) Karakitsou, K. E.; Verykios, X. E. *Journal of Catalysis* **1992**, *134*, 629.

(4) Domen, K.; Naito, S.; Onishi, T.; Tamaru, K. *Chemical Physics Letters* **1982**, *92*, 433.

(5) Inoue, Y.; Asai, Y.; Sato, K. *Journal of the Chemical Society-Faraday Transactions* **1994**, *90*, 797.

(6) Yoshimura, J.; Ebina, Y.; Kondo, J.; Domen, K.; Tanaka, A. *Journal of Physical Chemistry* **1993**, *97*, 1970.

(7) Inoue, Y.; Kubokawa, T.; Sato, K. *Journal of Physical Chemistry* **1991**, *95*, 4059.

(8) Bolton, J. R. *Solar Energy* **1996**, *57*, 37.

(9) Ashokkumar, M. *International Journal of Hydrogen Energy* **1998**, *23*, 427.

(10) Ashokkumar, M.; Maruthamuthu, P. *International Journal of Hydrogen Energy* **1991**, *16*, 591.

(11) Amouyal, E. *Solar Energy Materials and Solar Cells* **1995**, *38*, 249.

(12) Fujishima, A.; Honda, K. *Nature (London, United Kingdom)* **1972**, *238*, 37.

(13) Kudo, A.; Kato, H.; Tsuji, I. *Chemistry Letters* **2004**, *33*, 1534.

(14) Buxton, G. V.; Greenstock, C. L.; Helman, W. P.; Ross, A. B. *Journal of Physical and Chemical Reference Data* **1988**, *17*, 513.

(15) Shangguan, W. F.; Yoshida, A. *Journal of Physical Chemistry B* **2002**, *106*, 12227.

(16) Koca, A.; Sahin, M. *International Journal of Hydrogen Energy* **2002**, *27*, 363.

(17) Milczarek, G.; Kasuya, A.; Mamykin, S.; Arai, T.; Shinoda, K.; Tohji, K. *International Journal of Hydrogen Energy* **2003**, *28*, 919.

(18) Roy, A. M.; De, G. C. *Journal of Photochemistry and Photobiology a-Chemistry* **2003**, *157*, 87.

(19) Dewitt, R.; Kirschdemesmaeker, A. *Applied Physics Letters* **1984**, *45*, 146.

(20) Zhang, W. U.; Zhong, Y.; Fan, J.; Sun, S. Q.; Tang, N.; Tan, M. Y.; Wu, L. M. *Science in China Series B-Chemistry* **2003**, *46*, 196.

(21) Linkous, C. A.; Muradov, N. Z.; Ramser, S. N. *International Journal of Hydrogen Energy* **1995**, *20*, 701.

(22) Naman, S. A.; Almishhadani, N. H.; Alshamma, L. M. *International Journal of Hydrogen Energy* **1995**, *20*, 303.

(23) Chen, F.; Zhu, Y. P.; Ma, H. L.; Bo, Z. L.; Zhang, J. L. *Acta Physico-Chimica Sinica* **2004**, *20*, 1292.

(24) Zhang, J. L.; Xiao, M.; Liu, Z. M.; Han, B. X.; Jiang, T.; He, J.; Yang, G. Y. *Journal of Colloid and Interface Science* **2004**, *273*, 160.

(25) Innocenti, M.; Cattarin, S.; Loglio, F.; Cecconi, T.; Seravalli, G.; Foresti, M. L. *Electrochimica Acta* **2004**, *49*, 1327.

(26) Yoshimura, J.; Tanaka, A.; Kondo, J. N.; Domen, K. *Bulletin of the Chemical Society of Japan* **1995**, *68*, 2439.

(27) Shangguan, W. F.; Yoshida, A. *Solar Energy Materials and Solar Cells* **2001**, *69*, 189.

(28) Shangguan, W.; Yoshida, A. *Journal of Physical Chemistry B* **2002**, *106*, 12227.

(29) Darwent, J. R.; Porter, G. *Journal of the Chemical Society, Chemical*

Communications **1981**, 145.

(30) Borgarello, E.; Kalyanasundaram, K.; Graetzel, M.; Pelizzetti, E. *Helvetica Chimica Acta* **1982**, *65*, 243.

(31) Meissner, D.; Memming, R.; Kastening, B. *Solar Energy R&D in the European Community, Series D: Photochemical, Photoelectrochemical and Photobiological Processes* **1983**, *2*, 110.

(32) Meissner, D.; Memming, R.; Kastening, B. *Chemical Physics Letters* **1983**, *96*, 34.

(33) Buehler, N.; Meier, K.; Reber, J. F. *Journal of Physical Chemistry* **1984**, *88*, 3261.

(34) Serpone, N.; Borgarello, E.; Graetzel, M. *Journal of the Chemical Society, Chemical Communications* **1984**, *6*, 342.

(35) Kakuta, N.; Park, K. H.; Finlayson, M. F.; Ueno, A.; Bard, A. J.; Campion, A.; Fox, M. A.; Webber, S. E.; White, J. M. *Journal of Physical Chemistry* **1985**, *89*, 732.

(36) Ueno, A.; Kakuta, N.; Park, K. H.; Finlayson, M. F.; Bard, A. J.; Campion, A.; Fox, M. A.; Webber, S. E.; White, J. M. *Journal of Physical Chemistry* **1985**, *89*, 3828.

(37) Furlong, D. N.; Grieser, F.; Hayes, D.; Hayes, R.; Sasse, W.; Wells, D. *Journal of Physical Chemistry* **1986**, *90*, 2388.

(38) Kolts, J. H. Photochemical production of hydrogen from hydrogen sulfide; (Phillips Petroleum Co., USA). 1986, pp. 7.

(39) Matsumura, M.; Saho, Y.; Tsubomura, H. *NATO ASI Series, Series C: Mathematical and Physical Sciences* **1986**, *174*, 581.

(40) Reber, J. F.; Rusek, M. *Journal of Physical Chemistry* **1986**, *90*, 824.

(41) Kobayashi, J.; Kitaguchi, K.; Tanaka, H.; Tsuiki, H.; Ueno, A. *Journal of the Chemical Society-Faraday Transactions I* **1987**, *83*, 1395.

(42) Matsumura, M.; Tsubomura, H. *Journal of the Electrochemical Society* **1987**, *134*, C462.

(43) Mayo, P. d.; Wenska, G. *Tet. Lett.* **1987**, *43*, 1661.

(44) Muradov, N. Z.; Rustamov, M. I.; Guseinova, A. D.; Bazhutin, Y. V. *Reaction Kinetics and Catalysis Letters* **1987**, *33*, 279.

(45) Muradov, N. Z.; Rustamov, M. I.; Guseinova, A. D.; Bazhutin, Y. V. *Reaction Kinetics and Catalysis Letters* **1987**, *33*, 279.

(46) Vucemilovic, M. I.; Vukelic, N.; Rajh, T. *Journal of Photochemistry and Photobiology, A: Chemistry* **1988**, *42*, 157.

(47) Bahnemann, D. W.; Kormann, C.; Hoffmann, M. R. *J. Phys. Chem.* **1987**, *91*, 3789.

(48) Hoffman, A. J.; Carraway, E. R.; Hoffmann, M. R. *Environ. Sci. Technol.* **1994**, *28*, 776.

(49) Hoffman, A. J.; Mills, G.; Yee, H.; Hoffmann, M. R. *Journal of Physical Chemistry* **1992**, *96*, 5546.

(50) Hoffman, A. J.; Yee, H.; Mills, G.; Hoffmann, M. R. *Journal of Physical Chemistry* **1992**, *96*, 5540.

(51) Aparisi, A.; Fornes, V.; Marquez, F.; Moreno, R.; Lopez, C.; Meseguer, F. *Solid-State Electronics* **1996**, *40*, 641.

(52) Liu, X. S.; Iu, K. K.; Thomas, J. K. *Chemical Physics Letters* **1992**, *195*, 163.

(53) Liu, X. S.; Lu, K. K.; Thomas, J. K. *Journal of the Chemical Society-Faraday Transactions* **1993**, *89*, 1861.

(54) Fluckiger, U.; Arend, H.; Oswald, H. R. **1977**, *56*, 575.

(55) Domen, K.; Kudo, A.; Shibata, M.; Tanaka, A.; Maruya, K.; Onishi, T. **1986**, 1706.

(56) Fischer, C. H.; Weller, H.; Katsikas, L.; Henglein, A. *Langmuir* **1989**, *5*, 429.

(57) Fischer, C. H.; Lilie, J.; Weller, H.; Katsikas, L.; Henglein, A. *Ber. Bunsen-Ges. Phys. Chem. Chem. Phys.* **1989**, *93*, 61.

(58) Henglein, A.; Gutiérrez, M. *Ber. Bunseges. Phys. Chem.* **1983**, *87*, 852.

(59) Henglein, A. *Chemical Reviews* **1989**, *89*, 1861.

(60) Duran, J. D. G.; Guindo, M. C.; Delgado, A. V.; GonzalezCaballero, F. *Journal of Colloid and Interface Science* **1997**, *193*, 223.

(61) Guindo, M. C.; Zurita, L.; Duran, J. D. G.; Delgado, A. V. *Materials Chemistry and Physics* **1996**, *44*, 51.

(62) Liu, J. C.; Huang, C. P. *Langmuir* **1992**, *8*, 1851.

(63) Nicolau, Y. F.; Menard, J. C. *Journal of Colloid and Interface Science* **1992**, *148*, 551.

(64) Hoffman, A. J.; Mills, G.; Yee, H.; Hoffmann, M. R. *J. Phys. Chem.* **1992**, *96*, 5546.

(65) He, Y. J.; Hu, Y. Positron-Annihilation in Cd+2 Ion-Exchanged and Cds Loaded Zeolite-Y. In *Zeolites and Related Microporous Materials: State of the Art 1994*, 84, 2295.

(66) Li, B. H.; Wang, L. J.; Jin, Q. G.; Guo, Z. Y.; Tang, S. X.; Ding, D. T. *Journal of Porous Materials* **2002**, *9*, 287.

(67) Peng, H.; Liu, S. M.; Ma, L.; Lin, Z. J.; Wang, S. J. *Journal of Crystal Growth* **2001**, *224*, 274.

(68) Chen, W.; Wang, Z. G.; Lin, L. Y. *Journal of Luminescence* **1997**, *71*, 151.

(69) Jentys, A.; Grimes, R. W.; Gale, J. D.; Catlow, C. R. A. *Journal of Physical Chemistry* **1993**, *97*, 13535.

(70) Herron, N.; Wang, Y.; Eddy, M. M.; Stucky, G. D.; Cox, D. E.; Moller, K.; Bein, T. *Journal of the American Chemical Society* **1989**, *111*, 530.

(71) Wang, Y.; Herron, N. *Journal of Physical Chemistry* **1988**, *92*, 4988.

(72) Wang, Y.; Herron, N. *Journal of Physical Chemistry* **1987**, *91*, 257.

(73) Resch, U.; Eychmuller, A.; Haase, M.; Weller, H. *Langmuir* **1992**, *8*, 2215.

(74) Lakowicz, J. R. *Principles of Fluorescence Spectroscopy*; Kluwer Academic/Plenum: New York, 1999.

(75) Wang, Y.; Herron, N. *Journal of Physical Chemistry* **1991**, *95*, 525.

(76) Herron, N.; Wang, Y.; Eckert, H. *Journal of the American Chemical Society* **1990**, *112*, 1322.

(77) Yeshchenko, O. A.; Dmitruk, I. M.; Koryakov, S. V.; Pundyk, I. P.; Barnakov, Y. A. *Solid State Communications* **2005**, *133*, 109.

(78) Yu, Z. H.; Li, J. B.; O'Connor, D. B.; Wang, L. W.; Barbara, P. F. *Journal of Physical Chemistry B* **2003**, *107*, 5670.

(79) Liu, S. M.; Xu, Z.; Wageh, H.; Xu, X. R. *Spectroscopy and Spectral Analysis* **2002**, *22*, 908.

(80) Li, J. B.; Xia, J. B. *Physical Review B* **2000**, *62*, 12613.

(81) Woggon, U.; Saleh, M.; Uhrig, A.; Portune, M.; Klingshirn, C. *Journal of Crystal Growth* **1994**, *138*, 988.

(82) Korgel, B. A.; Monbouquette, H. G. *Journal of Physical Chemistry B* **1997**, *101*,

5010.

(83) Davis, A. P.; Huang, C. P. *Water Research* **1991**, *25*, 1273.

(84) Tang, W. Z.; Huang, C. P. *Chemosphere* **1995**, *30*, 1385.

(85) Davis, A. P.; Hsieh, Y. H.; Huang, C. P. *Chemosphere* **1994**, *28*, 663.

(86) Hsieh, Y. H.; Huang, C. P.; Davis, A. P. *Chemosphere* **1993**, *27*, 721.

(87) Hsieh, Y. H.; Huang, C. P.; Davis, A. P. *Chemosphere* **1992**, *24*, 281.

(88) Hsieh, Y. H.; Huang, C. P. *Colloids and Surfaces* **1991**, *53*, 275.

(89) Henglein, A. *Berichte der Bunsen-Gesellschaft* **1982**, *86*, 301.

(90) Hatchard, C. G.; Parker, C. A. *Proc. Roy. Soc. (London)* **1956**, *A235*, 518.

(91) Calvert, J. G.; Pitts, J. N. *Photochemistry*, 1966.

(92) Cornu, C. J. G.; Colussi, A. J.; Hoffmann, M. R. *Journal of Physical Chemistry B* **2001**, *105*, 1351.

(93) Cornu, C. J. G.; Colussi, A. J.; Hoffmann, M. R. *Journal of Physical Chemistry B* **2003**, *107*, 3156.

(94) Park, S. W.; Huang, C. P. *Journal of Colloid and Interface Science* **1987**, *117*, 431.

(95) De, G. C.; Roy, A. M. *Journal of Surface Science and Technology* **1999**, *15*, 147.

(96) Daskalakis, K. D.; Helz, G. R. *Environmental Science & Technology* **1992**, *26*, 2462.

(97) Licht, S.; Longo, K.; Peramunage, D.; Forouzan, F. *Journal of Electroanalytical Chemistry* **1991**, *318*, 111.

(98) Licht, S.; Manassen, J. *Journal of the Electrochemical Society* **1987**, *134*, 918.

(99) Licht, S.; Forouzan, F.; Longo, K. *Analytical Chemistry* **1990**, *62*, 1356.

(100) Schoonen, M. A. A.; Barnes, H. L. *Geochimica Et Cosmochimica Acta* **1988**, *52*, 649.

(101) Myers, R. J. *Journal of Chemical Education* **1986**, *63*, 687.

(102) Migdisov, A. A.; Williams-Jones, A. E.; Lakshtanov, L. Z.; Alekhin, Y. V. *Geochimica Et Cosmochimica Acta* **2002**, *66*, 1713.

(103) Meyer, B.; Ward, K.; Koshlap, K.; Peter, L. *Inorganic Chemistry* **1983**, *22*, 2345.

(104) Park, S. W.; Huang, C. P. *Journal of Colloid and Interface Science* **1987**, *117*, 431.

(105) Parks, G. A. *Chemical Reviews* **1965**, *65*, 177.

(106) Matijevic, E.; Wilhelmy, D. M. *Journal of Colloid and Interface Science* **1982**, *86*, 476.

(107) Faust, B. C.; Hoffmann, M. R.; Bahnemann, D. W. *Journal of Physical Chemistry* **1989**, *93*, 6371.

(108) Albers, C. *Zeitschrift fuer Physikalische Chemie (Leipzig)* **1968**, *237*, 278.

(109) Bontinck, W.; Dekeyser, W. *Naturwissenschaften* **1956**, *43*, 323.

(110) Davidson, R. S.; Willsher, C. J. *Journal of the Chemical Society, Dalton Transactions: Inorganic Chemistry (1972-1999)* **1981**, 833.

(111) Davidson, R. S.; Willsher, C. J. *Faraday Discussions of the Chemical Society* **1981**, *70*, 177.

(112) Gisolf, J. H. *Physica (The Hague)* **1939**, *6*, 84.

(113) Guntz, A. A. *Annali di Chimica Applicata* **1926**, *5*, 363.

(114) Lenard, P. *Annalen der Physik (Berlin, Germany)* **1922**, *68*, 553.

(115) Merz, W. J. *Helvetica Physica Acta* **1957**, *30*, 244.

(116) Niekisch, E. A.; Pflaum, U.; Rompe, R. *Zeitschrift fuer Physikalische Chemie (Leipzig)* **1956**, *205*, 146.

(117) Schleede, A.; Herter, M. *Zeitschrift fuer Elektrochemie und Angewandte Physikalische Chemie* **1923**, *29*, 411.

(118) Schleede, A.; Herter, M.; Kordatzki, W. *Z. physik. Chem.* **1923**, *106*, 386.

(119) Shionoya, S.; Watanabe, K. *Bull. Chem. Soc. Japan* **1957**, *30*, 118.

(120) Sviszt, P. *Acta Physica Polonica* **1964**, *26*, 823.

(121) Stroyuk, A. L.; Shvalagin, V. V.; Raevskaya, A. E.; Korzhak, A. V.; Kuchmii, S. Y. *Theoretical and Experimental Chemistry (Translation of Teoreticheskaya i Eksperimental'naya Khimiya)* **2003**, *39*, 341.

(122) Job, A.; Ernschwiller, G. *Compt. rend.* **1923**, *177*, 313.

(123) Markham, M. C.; Barry, J.; Iava, M.; Haddad, J. *Journal of Physical Chemistry* **1957**, *61*, 1665.

(124) Gutierrez, M.; Henglein, A. *Berichte der Bunsen-Gesellschaft* **1983**, *87*, 474.

(125) Shiragami, T.; Ankyu, H.; Fukami, S.; Pac, C.; Yanagida, S.; Mori, H.; Fujita, H. *Journal of the Chemical Society-Faraday Transactions* **1992**, *88*, 1055.

(126) Reber, J. F.; Meier, K. *Journal of Physical Chemistry* **1984**, *88*, 5903.

(127) Ohtani, B.; Kusakabe, S.; Okada, K.; Tsuru, S.; Nishimoto, S.; Amino, Y.; Izawa, K.; Nakato, Y.; Matsumura, M.; Nakaoka, Y.; Nosaka, Y. **2001**, 201.

(128) Henglein, A.; Lindig, B.; Westerhausen, J. *Journal of Physical Chemistry* **1981**, *85*, 1627.

(129) Guan, G.; Kida, T.; Kusakabe, K.; Kimura, K.; Fang, X.; Ma, T.; Abe, E.; Yoshida, A. *Chemical Physics Letters* **2004**, *385*, 319.

(130) Hayashi, H.; Hakuta, Y.; Kurata, Y. **2004**, *14*, 2046.

(131) Ewart, M.; Biaggio, I.; Zgonik, M.; Gunter, P. **1994**, *49*, 5263.

(132) Kesselman, J. M.; Weres, O.; Lewis, N. S.; Hoffmann, M. R. *Journal of Physical Chemistry B* **1997**, *101*, 2637.

(133) Yariv, A.; Orlov, S. S.; Rakuljic, G. A. **1996**, *13*, 2513.

(134) Nel, J. M.; Auret, F. D.; Wu, L.; Legodi, M. J.; Meyer, W. E.; Hayes, M. **2004**, *100*, 270.